THE RELATIVE OPTICAL DENSITY OF GLYCOGEN PHOSPHORYLASE AND ASTROCYTIC GFAP PROFILE IN THE HIPPOCAMPUS IN A RAT MODEL OF ALZHEIMER'S DISEASE AT THE PRETANGLE STAGE.

By © Abass Haruna

A Thesis Submitted

to the School of Graduate Studies in partial fulfillment of the

requirements for the degree of

Master of Science, Department of Psychology, Faculty of Science

Memorial University of Newfoundland

March 2024

St. John's, Newfoundland and Labrador

Abstract

Glycogen, a stored form of glucose, is involved in the brain's metabolism, especially in pathological conditions such as Alzheimer's Disease (AD). AD is an age-associated neurodegenerative disorder linked with cognitive deficits and increases in astrocyte reactivity (neuroinflammation). AD is preceded by the accumulation of hyperphosphorylated tau in the locus coeruleus (LC) nucleus of the brainstem as identified in Braak's pretangle stages. The current study examined relative changes in activity of glycogen phosphorylase (GP), the enzyme that breaks down glycogen for metabolic use by neurons in the hippocampus of a rat model of Braak's LC-originated pretangle stage. An htauE14 transgene was infused in the LC of TH-Cre older rats (~20-month p.i) using a viral vector. Chimeric procedures for GP activity were performed with matched experimental and control brain tissue. Relative optical density (ROD) measurements of GP and astrocyte glial fibrillary acidic protein (GFAP) profile of rats in the experimental group (LC-htauE14 infused) were compared with control rats (rats without htauE14 infusion). Repeated measures analyses revealed that LC-htauE14 infusion did not alter the GP levels (aGP, tGP, and ratio) and the astrocyte GFAP expression in the hippocampus of these rats at the pretangle stage of AD. There were no sex-dependent alterations detected. However, various subregions within the hippocampal DG, CA3 and CA1 showed different levels of GP activity and GFAP profiles regardless of sex and condition. These findings indicate that GP and GFAP ROD are not altered at the pretangle stage of AD, suggesting the potential existence of compensatory mechanisms in addressing energy demands at the early phases of AD.

General Summary

Alzheimer's disease (AD) is a condition marked by memory loss and distinct changes in brain cells. Prior to the onset of AD, there is an abnormal protein called phosphorylated tau, which first develops in locus coeruleus (LC) within the brainstem. AD is a type of dementia demanding increased energy and substantially impacts the hippocampus, a key memory-associated brain region. Glycogen, serving as a reserve energy source, becomes utilized during intensified energy-demanding activities in the brain. This study examined glycogen activity within the hippocampus using a rat model (htauE14) mimicking this early AD stage. I examined the activity of the enzyme glycogen phosphorylase (GP), which is involved in breaking down glycogen to supply neurons with energy. No evident effect of this abnormal protein (htauE14) on GP activity in the hippocampal regions was found. Additionally, no observable changes occurred in astrocytes, where GP is primarily located, in the rats. These findings imply that the brain might employ alternative mechanisms to manage energy requirements distinct from glycogen utilization during the initial stages of AD.

Co-Authorship Statement

In this co-authorship statement, I affirm that this thesis includes materials derived from collaborative research efforts. Specifically, the surgeries and infusions on rats were conducted in collaboration with Marie Wacef (former MSc student) and Ella Chiniros (research assistant) under the guidance of Dr. Susan Walling. Ella Chiniros also carried out rat anesthesia and euthanasia. Nevertheless, I take responsibility for the primary contributions, including experimental design, data analysis, interpretation, and writing.

Acknowledgement

I am profoundly grateful to the Almighty God for His guidance and blessings, which have been the cornerstone of my academic journey.

I would like to express my sincere appreciation to Dr. Susan Walling. Gaining admission to the University and travelling in the midst of a pandemic was undoubtedly challenging. Dr. Walling has been an invaluable resource for me on my journey. Even before I travelled here, she remained a constant source of support as I made tough decisions I could not have made without her help. Dr. Walling has been an incredibly supportive, encouraging, and pivotal supervisor for me in my academic journey and beyond. Thank you for reading my thesis drafts and providing suggestions. It has been a great privilege working with and being mentored by her.

I extend my heartfelt gratitude to Dr. Carolyn Walsh and Dr. Ashlyn Swift-Gallant for being part of my supervisory committee. Thank you for your insightful feedback and contributions to this work. Thank you to all the members of WallingNeuroLab whose collaboration and assistance have been instrumental in the success of this research endeavor.

I am indebted to my family for their unconditional love, understanding, and unwavering support throughout this course. Lastly, to my friends, whose unflinching support and encouragement have been a constant source of motivation, thank you for being there all the time.

Table of Contents

List of Figures

List of Abbreviations

AD	Alzheimer's disease
AAV	Adeno-associated virus
AC-3	Active caspase 3
aGP	Active glycogen phosphorylase
ANLS	Astrocyte-neuron-lactate shuttle
ATP	Adenosine triphosphate
bGP	Inactive glycogen phosphorylase
CA1	Cornu ammonis 1
CA1 lacmol	Cornu ammonis 1 lacnosum moleculare
CA1 pyr	Cornu ammonis 1 pyramidal
CA1 rad	Cornu ammonis 1 radiatum
CA3	Cornu ammonis 3
CNS	Central nervous system
DAB	3,3'-Diaminobenzidine
DG	Dentate Gyrus
DG-GCL	Dentate gyrus- granule cell layer
DβH	Dopamine beta-hydroxylase
G-6-P	Glycogen-6-phosphate
GFAP	Glial fibrillary acidic protein
GFP	Green fluorescent protein
GLUT 1	Glucose transporter
GP	Glycogen Phosphorylase
HK	Hexokinase

htauE14	Pseudo-phosphorylated human tau
LC	Locus Coeruleus
LC-NE	Locus Coeruleus-Norepinephrine
LDH	Lactate dehydrogenase
MCI	Mild cognitive impairment
MAS	Malate aspartate shuttle
NA	Noradrenergic
NADH	Nicotinamide adenine nucleotide
NE	Norepinephrine
NET	Norepinephrine transporter
NFT	Neurofibrillary tangle
OGI	Oxygen glucose index
p.i	Post infusion
PPP	Pentose phosphate pathway
ROD	Relative optical density
S.C	Subcutaneous
SGZ	Subgranular zone
TCA cycle	Tricarboxylic acid cycle
tGP	Total glycogen phosphorylase
TH-Cre	Tyrosine hydroxylase cre-recombinase
3xTg	Triple transgenic
UTP	Uridine triphosphate

1. The Relative Optical Density of Glycogen Phosphorylase and Astrocytic GFAP Profile in the Hippocampus in a Rat Model of Alzheimer's Disease at Pretangle Stage.

The brain is one of the body's organs with the highest energy metabolism. Although it accounts for only 2% of body weight, it utilizes approximately 25% of total body glucose in the resting awake state (Sokoloff, 1999). Evidence indicates a significant rise in the brain's energy demands during pathological conditions such as Alzheimer's Disease (AD) (Brown et al., 2004; Swanson et al., 1992). Glycogen, a crucial energy source during low brain glucose levels, is regularly utilized to support normal brain function and high neuronal activities (Magistretti & Pellerin, 1996; Swanson et al., 1992). However, the alterations in glycogen metabolism during pathophysiological conditions (e.g. AD) are not yet well understood. This research outlined in this thesis examined relative changes in glycogen phosphorylase (GP) activity and glial fibrillary acidic protein (GFAP) expression in the hippocampus during a pretangle stage of AD.

1.1 The Scope of AD

Millions of people worldwide are impacted by a neurodegenerative condition called AD. AD is the most common form of dementia, accounting for approximately 60–80% of all dementia cases (Alzheimer Society, 2023; Hendrie et al., 1995). It is estimated that 50 million individuals have dementia globally, and this is expected to triple by the year 2050 (World Health Organization, 2021). After age 65, the prevalence of AD tends to double every five years, affecting about 50% of people over 85 (Evans et al., 1989). According to the Alzheimer Society of Canada (2023), in 2020, a total of 124,000 individuals in Canada were diagnosed with

dementia. Women comprised 61.8% of people living with dementia in this cohort in that year. Growing healthcare costs due to the ageing population have placed additional strains on society and individuals. Moreover, dementia places a heavy financial and medical burden on Canada, costing the country's economy and healthcare system more than $10.4 billion annually (Alzheimer Society of Canada, 2023).

AD is a degenerative neurological disease, characterized by generalized atrophy of the brain (Perry, 1999) and a decline in cognitive capacity, memory loss, and behavioral disturbances (Reisberg et al., 1982). It eventually results in severe cognitive impairment and death (Iqbal et al., 1987). Alois Alzheimer originally identified the first case of AD in 1906 (as reported in Glenner & Wong, 1984). Alzheimer's pathological analysis found atrophy and particular lesions that he defined as “paucity of cells in the cerebral cortex and buildup of filaments between nerve cells” (as translated in Alzheimer et al., 1995). His findings included the deposition of abnormal proteins called amyloid plaques and intracellular accumulation of abnormal and misfolded protein, known as neurofibrillary tangles (NFTs) in the brain of a 55-year patient with advanced dementia (Glenner & Wong, 1984; Zilka & Novak, 2006).

1.1.2 Tau Protein

Accumulated and misfolded tau protein is considered one of the hallmarks of AD. According to Drechsel et al. (1992), tau works intracellularly to facilitate microtubule organization, stabilization and assembly, which is crucial for the development of axons and dendrites in neurons. The discovery of hyperphosphorylated tau as the main constituent of NFTs in the AD brain led to the established relationship between tau and neurodegenerative disorders in 1986 (Glenner & Wong, 1984; Iqbal et al., 1987). In AD, the tau changes, dissociating from

the microtubule and creates tangles which damage the axonal microtubules in neurons and hinder axonal transport (Iqbal et al., 2009). This may eventually result in cell death (Busser et al., 1998).

Although the precise initial underlying cause of AD is still unknown, several risk factors exist. The incidence of AD increases with age, making aging the most significant risk factor (Hendrie et al., 1995). Genetics, sex, family history, brain injuries, and long-term medical conditions such as diabetes, and hypertension are additional risk factors (Hendrie et al., 1995).

1.2 Braak's Staging of Tau Pathology in AD

Braak et al. (2011) proposed five pretangle stages to explain the changes that occur before the appearance of tangles in AD. According to the authors, during the pretangle stage, the abnormally phosphorylated tau remains soluble, and symptoms of the disease have not appeared. Pretangle material is initially localized to the locus coeruleus (LC) processes in the first stage (stage a) as described previously (Braak & Braak, 1991; Del Tredici et al., 2002). The LC is the primary noradrenergic nucleus (containing norepinephrine; NE) located in the brainstem, which, has been linked to the pathophysiology of AD (Bondareff et al., 1987; Mathews et al., 2002). In the second stage (stage b), pretangle material spreads to the soma and dendrites. And by stage c, other brainstem nuclei become affected. Hyperphosphorylated tau is present at the end of LC axons in the transentorhinal cortex at stage 1a. In stage 1b, pretangle material covers the transentorhinal cortex's soma and pyramidal cell processes.

Braak's staging of tangle (NFT) pathology advances through six stages, beginning in the entorhinal cortex and progressing throughout the neocortex. Braak and Braak (1991) state that tangles appear in the entorhinal cortex during the first stage, which later spreads to the hippocampus and amygdala in the second stage. The neocortex starts to show signs of tangles in the third stage. By the fourth and fifth stages, abnormal tau has spread across the neocortex,

causing neuronal death and synaptic loss. The last stage is marked by significant cognitive decline and dementia and involves the total loss of neocortical function (Braak & Braak, 1991).

Moreover, Braak et al. (2011) investigated more than 2000 post-mortem brains from individuals aged 1 to 100 and reported that abnormal tau pathology occurs first in the LC within the brainstem before spreading systematically throughout the cortex. It was determined that the severity of cognitive impairments varied with age and disease stage, with older people reporting severe deficits at later phases of the disease. Creating an animal model resembling Braak's pretangle stages can help in AD early diagnosis, intervention techniques, and treatment.

1.2.1 Animal Studies of Braak's Pretangle Stage Model

Animal research has contributed to our understanding of the pretangle stages of tau abnormality, which were first identified by Braak et al. (2011). Ghosh et al. (2019) and Omoluabi et al. (2021) successfully replicated these stages in rat models, making a substantial addition to the AD research field and laying the foundation for further studies in this area.

Ghosh et al. (2019) investigated the mechanism by which persistently phosphorylated tau expression in the LC triggers initial deficits in associative olfactory learning and memory. This model involved the introduction of a human pseudophosphorylated tau (htauE14) gene into the LC via an adenoassociated viral vector (AAV), inducing the early expression of the human soluble hyperphosphorylated pretangle stages in 2–3-month-old TH-Cre$^{+/-}$ rats. Their study involved various assessments, including simple and complex odor discriminations and the spread of htau throughout the LC axons, LC neurons and fiber densities in the primary olfactory cortex in these rats. They further linked behavioural deficits to LC pathology in rats at different stages.

The results demonstrated that htauE14 rapidly co-expressed in LC neurons. Subsequently, htauE14 was localized to LC cell bodies and dendrites, mimicking the pathology

seen in pretangle AD (Ghosh et al. 2019). After 6 weeks, htauE14 began to spread along LC axons in the direction of forebrain targets. By 12 weeks, it had reached the olfactory bulb and many cortical areas, including the hippocampus and piriform cortex. Subsequent analysis conducted 3-6 months post-infusion on adult rats (5-6 months old) revealed no deficiencies in odor discrimination. Though there was no observable loss of LC cells at 7–8 months post-infusion, htauE14 rats exhibited difficulties in complex, similar odor discrimination learning. Compared to controls, there was a substantial loss of norepinephrine transporter (NET) labelled fiber within the piriform cortex of the htauE14 rats (Ghosh et al., 2019).

Comparing the effects of early-onset versus late-onset tau pathology in the LC, rats infused at older ages showed more severe behavioural impairments (6 months post-infusion) in relation to younger infused rats (Ghosh et al., 2019). The older infused rats displayed impaired learning in the initial simple, dissimilar odor discrimination, accompanied by significant LC cell loss and decreased NET and the norepinephrine synthesizing enzyme dopamine-β-hydroxylase (DBH) labelled fiber density in the piriform cortex. The astrocyte marker GFAP did not show any co-localization with GFP cells, and no evidence of tangles via Thioflavin-S staining was observed. However, these older animals exhibited transneuronal spread and neuron-to-microglia spread (Ghosh et al., 2019).

Later, in an optogenetic study, Omoluabi et al. (2021) employed gene-insertion methods to activate specific genes in LC neurons. To seed pretangle tau in the LC and activate LC noradrenergic neurons, the researchers utilized TH-CRE rats and injected dual CRE-dependent AAV-htauE14, while the other contained light-sensitive channel rhodopsin 2 (ChR2). Subsequently, rats were implanted with optical cannula 5-months after AAV infusion and

received daily light stimulations for 6 weeks. These stimulations encompassed phasic and tonic LC activation patterns (Omoluabi et al., 2021).

Omoluabi et al. (2021) also conducted behavioral assessments approximately 9 to 10 months post AAV infusion evaluating stress/anxiety levels using open field, marble burying, and elevated plus maze tests. Tonic-stimulated htauE14 rats displayed heightened anxiety and increased stress levels. Conversely, phasic-stimulated htauE14 rats showed comparable performance to control rats, indicating a potential anxiolytic effect of phasic LC activation.

Subsequent histological and immunohistochemical analyses (12 months post-AAV infusion) revealed no loss of LC cells but increased apoptosis marker, active caspase 3 (AC-3) in tonic-stimulated htauE14 rats. DBH and NET as noradrenergic fiber markers showed decreased fiber density in brain regions crucial for spatial and olfactory pattern separation (piriform cortex and hippocampal dentate gyrus) due to pretangle tau seeding. However, phasic LC stimulation stopped the LC fiber degeneration (Omoluabi et al., 2021).

Furthermore, the study explored the influence of LC activation patterns on pretangle tau spread by using HT7 as a marker (Omoluabi et al., 2021). It was observed that pretangle tau had spread to various subcortical regions such as the raphe nuclei, pontine tegmental nuclei and the substantia nigra. However, the pretangle tau pattern and GFP cell densities did not significantly differ among groups. AT8 measurement of tau phosphorylation patterns were not observed outside the brainstem and Thioflavin-S staining did not reveal the presence of tau tangles in any brain areas (Omoluabi et al., 2021).

These animal studies underscore the critical role of LC in pretangle tau pathology and its implications for cognitive deficits in AD, offering insights into potential therapeutic interventions targeting LC neuron activity.

1.3 Brain Energy Metabolism and AD

In humans, glucose metabolism occurs predominantly in the brain. The activity of neurons heavily depends on glucose as its primary energy source. Evidence consistently suggests that disrupted glucose metabolism is associated with AD. There is a reported 17-24% reduced cerebral glucose metabolism revealed by positron emission tomographic (PET) technique in senile dementia of the Alzheimer type (SDAT) patients compared to older controls (de Leon et al., 1983). These declines are more pronounced in regions particularly affected by AD, such as the posterior cingulate, frontal, parietal, and temporal cortices (Braak & Braak, 1991; Delacourte et al., 1999; de Leon, 1983).

1.4 Cerebral Metabolic Pathways

The metabolism of glucose in the brain is a complex process involving multiple cell types and competitive metabolic pathways, essential for meeting the energy requirements associated with neuronal activation. Glucose transport across the blood-brain barrier is mediated by the glucose transporter GLUT-1, primarily expressed in astrocytes and the capillary endothelium (Morgello et al., 1995). Astrocytes serve as intermediaries between glucose uptake from the blood and delivery to neurons. Glucose is then phosphorylated by hexokinase (HK) inside the astrocyte, forming glucose-6-phosphate (G-6-P) (see Figure 1). The pentose phosphate pathway (PPP) is responsible for G-6-P metabolism and NADPH generation, while glycolysis produces pyruvate, NADH, and ATP (Dienel & Cruz, 2003).

Astrocytes can convert G-6-P into glycogen, a glucose polymer that serves as an energy reserve in the brain (Nelson et al., 1984). Evidence suggests that glycogen mobilization in astrocytes is associated with functional memory through glutamate synthesis and lactate shuttling

between astrocytes and neurons (Swanson et al., 1992). During increased neuronal activity, glycogen is broken down by glycogen phosphorylase (GP) into lactate (glycogenolysis) to fuel neuronal metabolism. Astrocytes take glucose from blood vessels via GLUT1 and convert it to lactate through aerobic glycolysis (Dienel & Rothman, 2019, see Figure 1).

Lactate serves as an energy substrate within the brain via its conversion into pyruvate (Morgello et al., 1995; Pellerin & Magistretti, 1994) and then enters the tricarboxylic acid cycle (TCA cycle) for oxidative metabolism to produce ATP and support the energy demands of neurons (Pellerin & Magistretti, 1994; Magistretti & Pellerin, 1996). Newman et al. (2011) and Suzuki et al. (2011) highlighted that the primary role of lactate may be metabolic, thereby supporting energy-demanding activities of learning and memory.

1.4.1 Astrocyte-Neuron Lactate Shuttle (ANLS)

The astrocyte-neuron lactate shuttle (ANLS), a hypothesis proposed by Pellerin and Magistretti (1994), postulates that coordinated roles in the creation of long-term memories are played by astrocyte glycolysis and neuronal oxidation via the transport of lactate. The ANLS model contends that astrocytes take up glucose from blood arteries and metabolize it through glycolysis, yielding lactate as a byproduct. This lactate is then released extracellularly and taken up by neurons, where it undergoes conversion to pyruvate (see Figure 1) with the help of the lactate dehydrogenase (LDH) enzyme (Morgello et al., 1995; Pellerin & Magistretti, 1994). Pyruvate enters the neuronal TCA cycle, producing ATP by oxidative phosphorylation to support energy demands (Dienel & Cruz 2003).

Glycogen synthesis uses 1 ATP equivalent (UTP) for each integration of a glucosyl unit into glycogen, requiring 2 ATP molecules. In contrast, glycogenolysis, the process of glycogen breakdown, generates a net of 3 ATP molecules, producing 1 ATP for every turn of a single

glucosyl unit (Figure 1). The benefit of storing glucose as glycogen is that it enables synthesis to occur when there is low energy demand, while breakdown can quickly fulfil rising ATP demands (Dienel & Cruz, 2003; Magistretti & Pellerin, 1996). The brain's distribution of energy and metabolic equilibrium depends on this glial-neuronal energy shuttle. It allows astrocytes, which have a high glycolytic capacity, to supply lactate to neurons, which have a higher oxidative metabolism (Magistretti & Pellerin, 1996). This cooperative process optimizes energy use and distribution across many cell types within the brain. However, further research is needed to understand the variations in neuronal activation, aerobic glycolysis, and lactate shuttling during aging and in conditions such as AD.

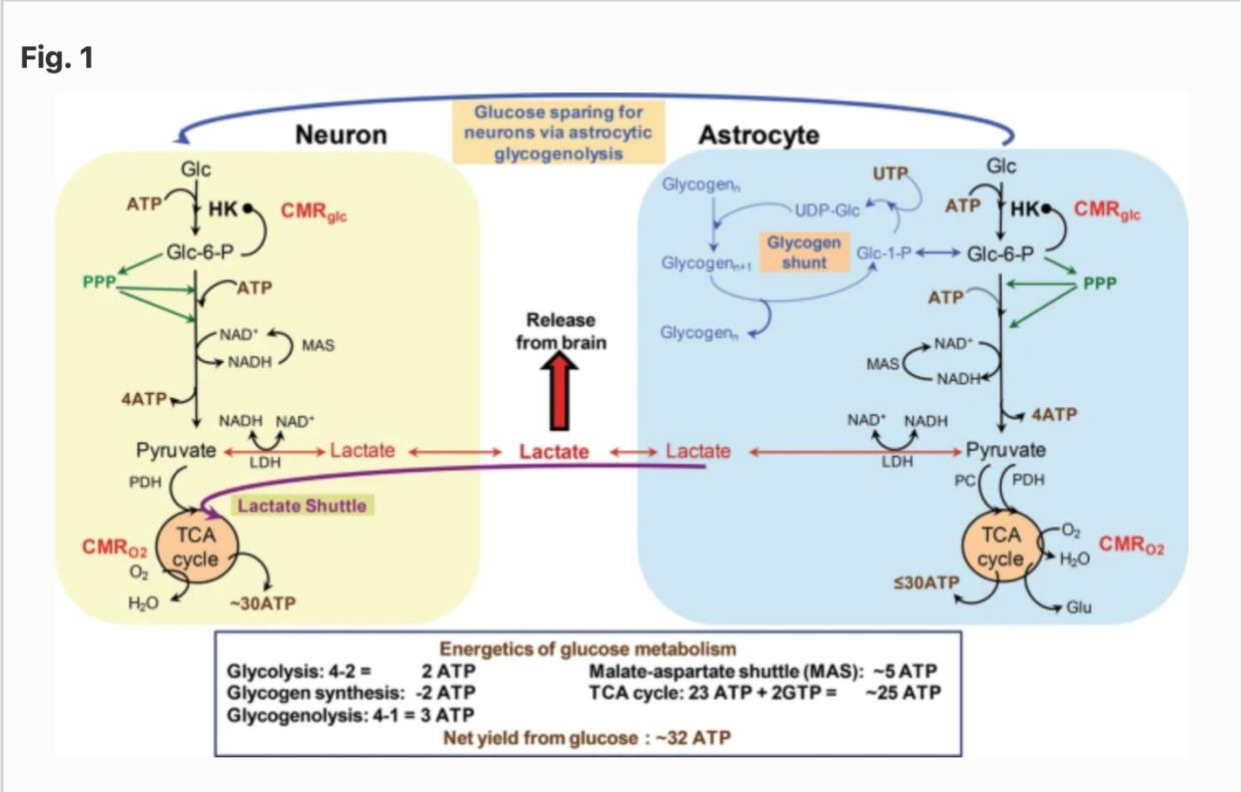

Figure 1: A schematic representation showing the many metabolic mechanisms and routes involved in the brain's use of glucose and glycogen (Image taken from Dienel & Rothman, 2019). It assumes that the glycolytic process breaks down glucose into pyruvate and ATP. The malate-aspartate shuttle (MAS) and the oxidative route contribute to producing extra ATP. The initial stage of glycolysis, the hexokinase (HK) reaction, is feedback inhibited by glucose-6-phosphate. The oxygen-glucose index (OGI) is used to quantify the stoichiometry of oxygen-to-glucose utilization. Some glucose-6-phosphate can enter the pentose phosphate shunt pathway, while most carbon re-enters the glycolytic pathway. Glycogen, predominantly found in astrocytes, can be synthesized and degraded to meet energy demands efficiently. Glycogen synthesis requires 1 ATP equivalent as UTP, while glycogenolysis has a net yield of 3 ATP, resulting in an overall gain of 1 ATP per turnover of 1 glucosyl unit. It also describes the role of pyruvate dehydrogenase and pyruvate carboxylase in astrocyte metabolism. The lactate shuttle is proposed to transfer lactate from astrocytes to neurons for oxidation. According to an alternative model by DiNuzzo et al. (2010), during brain engagement, glycogenolysis lessens the need for astrocytes to absorb glucose, potentially saving glucose for neuronal use.

1.5 Astrocytes and Glycogen

The most prevalent form of glial cell in the brain is astrocyte, which regulates brain homeostasis and neuronal activity (Brown et al., 2004; Chesler & Himwich, 1944; Magistretti et al., 1993). Neurological diseases arise due to disruptions in the delicate balance between neural cell damage, neuroprotection, and regeneration. Astrocytes, as homeostatic cells in the CNS, are consistently implicated in various neuropathologies (Giaume et al., 2007; Seifert et al., 2006). These cells are crucial in inflammation, responding to neuronal damage and cell death, which could be pertinent to AD (Sokoloff, 1999; Wilhelmson et al., 2006).

Glycogen, a branched glucose polymer, is stored by astrocytes (Magistretti et al., 1993) and used as an energy source in the brain (Brown et al., 2004). Initially, studies examining dogs experiencing insulin-induced hypoglycemia were done to better understand the role of brain glycogen under low blood glucose delivery conditions (Chesler & Himwich, 1944). For the first time, these experiments established a relationship between glycogen content and brain function, which showed that the glycogen levels noticeably dropped in brain areas with the highest metabolic activity. Later, Gibbs et al. (2006) also demonstrated the involvement of glycogen metabolism in higher brain functions. This study reported that pharmacological inhibition of glycogenolysis (the breakdown of glycogen) caused a decrease in memory consolidation in chickens.

Glycogen and astrocytes are closely related in the brain, with astrocytes responsible for glycogen storage and utilization to support neuronal energy supply and general brain function. Early research by Swanson et al. (1992) showed considerable glycogen stores in astrocytes, which serve as a crucial energy reserve during increased brain activity. Magistretti and Pellerin (1996) emphasized the significance of glycogen as an alternative source when glucose becomes

inadequate, with glycogen breakdown in astrocytes generating lactate to satisfy neuronal energy requirements. While Dienel and Cruz (2003) demonstrated the importance of astrocytic glycogen in preserving brain energy homeostasis, studies by Newman et al. (2011) and Suzuki et al. (2011) highlighted the importance of glycogen-derived lactate in astrocytes for memory processing and consolidation. These findings collectively emphasize the importance of glycogen metabolism in astrocytes, which affects neuronal energy supply and memory functions.

1.5.1 Glycogen Phosphorylase (GP)

The enzyme GP plays a role in converting glycogen into glucose-1-phosphate, which can then be used to produce energy. GP is expressed in astrocytes and neurons, with astrocytes expressing most of it (Swanson et al., 1992). GP occurs in two forms: phosphorylated form known as active GP (aGP) and dephosphorylated form known as inactive GP (bGP) (Cori & Cori, 1945; Fischer & Krebs, 1955). The total GP (tGP) is comprised of both aGP and bGP.

The link between advanced brain activity and glycogen metabolism was initially demonstrated by Gibbs et al. (2006). They demonstrated that memory consolidation during bead discrimination learning in young chicks was disturbed by blocking glycogenolysis in astrocytes with the use of 1,4-dideoxy-1,4-imino-D-arabinitol (DAB), a powerful inhibitor of glycogen phosphorylase (Gibbs et al., 2006).

One of the brain areas to be impacted early by AD is the hippocampus, which is essential for learning, memory, and cognitive function (Garcia-Alloza et al., 2006; Price & Morris, 1999). Research has revealed a connection between neurological conditions and astrocytic glycogen metabolism in the hippocampus. Walling et al. (2007) examined the alterations in GP in the pathological condition of severe seizures (epilepsy). Pilocarpine, a drug used to cause seizures in experimental settings, was administered to male rats as part of the study. The study examined

how an unremitting seizure episode may affect glycolytic energy demand in rats. The rats were examined at different intervals (one hour, one week, and one month) following a period of 'status epilepticus'- a serious seizure unremitting for periods of one hour or more (Walling et a., 2007). Results were contrasted with those of control animals who had saline injections. Relative optical density (ROD) measurements revealed that the condition caused a reduction in aGP primarily in the entorhinal cortex and hippocampus after one hour, while overall GP remained unchanged. However, it was discovered that both the aGP and tGP levels had increased in contrast to the control group after one week and one month (Walling et al., 2007). It is, therefore, imperative to investigate the GP changes that may occur under energy-demanding situations such as pretangle AD condition and how this may affect males and females differently.

1.6 The LC-NE System

Cells within the brainstem LC synthesize and release norepinephrine (NE) to forebrain structures. Research studies by Swanson et al. (1992), Gibbs et al. (2006) and Suzuki et al. (2011) revealed that the LC-NE signaling system regulates GP activity in astrocytes to produce lactate as an energy source for neurons. Additionally, NE is a neurotransmitter which can modulate the activity of GP in neurons and helps to control the brain's energy consumption (Gibbs et al., 2006).

Heneka et al. (2010) reported that the LC-NE system is crucial to the pathophysiology of AD. Early in the disease, LC neurons deteriorate, and NE levels are decreased in AD patients' brains (Heneka et al., 2010; Mathews et al., 2002). This lack of LC-NE signaling can contribute to decreased GP activity (Gibbs et al. (2006) consistent with altered glycogen metabolism in AD. Understanding the molecular mechanisms behind these regulatory processes can provide insights into the pathophysiology of AD and help develop novel therapeutic strategies.

1.7 Relationship among Astrocytes, Brain Metabolism and AD.

Astrocytes are glial cells that play various roles in the brain, including energy metabolism, controlling extracellular ion concentrations, absorbing and releasing neurotransmitters, and maintaining the blood-brain barrier (Matsui et al., 2012). Astrocytes play a crucial role in regulating energy metabolism in the brain through the preservation and usage of glycogen. The glycogen metabolism by astrocytes in the hippocampus serves as a source of energy for neurons during periods of high activity (Matsui et al., 2012).

In AD, the hippocampus is one area of the brain more prone to harm, and astrocyte dysfunction can contribute to this vulnerability.

In addition to glycogen metabolism, astrocytes control glycolysis and glucose uptake in the brain. According to Mosconi et al. (2009), there is evidence of poor energy production and decreased glucose metabolism in the brain of AD patients, which may contribute to cognitive deterioration. Due to the role that astrocytes play in the control of glucose uptake and utilization, they could contribute to this metabolic deficit.

Olabarria et al. (2010) have reported general astrocyte atrophy in the hippocampal area (CA1 and DG) of triple transgenic mice of AD (3xTg-AD). At an early age (6 months old), the study found decreased surface and volume of GFAP profiles in the DG, but this reduction appeared later (18 months) in the CA1. However, neither AD nor age altered the numerical astrocytic density in these mice.

The pathogenesis of AD is influenced by astrocyte morphological alterations and astrocytic malfunction through various processes such as glycogen metabolism and LC dysfunction. More investigation into the function of astrocytes in AD can shed new light on the creation of effective treatment options for this neurodegenerative disease.

1.8 Sex Differences in AD

Although there have been reports on differential rates of brain atrophy in various male and female brain regions of healthy aging, mild cognitive impairment (MCI), and AD subjects (Hua et al., 2010; Skup et al., 2011), biomarker studies have not been able to provide noticeable sex differences in the amyloid or NFT burden (Barnes et al., 2005; Shinohara et al., 2016), and levels of tau (Mattsson et al., 2017) in AD patients. Moreover, studies employing PET techniques also reported no substantial sex difference between male and female MCI subjects on tau aggregation (Johnson et al., 2016).

Among AD patients, the rate of cognitive deterioration in women is twice as fast as in men, as reported in the Alzheimer's Disease Neuroimaging Initiative study (Lin et al., 2015). In several studies (Filon et al., 2016; Gale et al., 2016; Malpetti et al., 2017; Tensil et al., 2018), female AD patients exhibit more profound cognitive decline than male patients, with more significant reductions seen in all cognitive domains and verbal and visuospatial performance. Additionally, there are observed sex differences in behavioral symptoms in AD patients. Women with AD are more likely to experience depressive symptoms and delusions than men with AD. On the other hand, men affected with AD are more likely to exhibit agitation and socially inappropriate behaviors than women (Karttunen et al., 2011; Kitamura et al., 2012; Mega et al., 1996).

Finally, while various AD transgenic mouse models have provided evidence of sex-specific effects in amyloid burden and cognitive impairments (Dubal et al., 2012), the influence of sex on tau hyperphosphorylation is still unclear (Yue et al., 2011). Despite several studies highlighting differences in male and female AD patients, very few studies have focused on sex-specific differences in energy metabolism. My literature search showed that few studies have

investigated sex differences in GP activity and astrocyte expression in AD. Given the sex differences in diagnosis rate and in symptomology, sex-specific therapies may need to be developed and may be more effective should the underlying mechanisms be found to differ between the sexes. As such, a better understanding of the molecular processes behind these sex differences is needed.

1.9 Focus of the Present Study

Alzheimer's disease was traditionally diagnosed based on clinical observations, such as age-related memory loss, cognitive deficits, and neuropathological findings, including post-mortem senile plaques and NFTs in neurons. Preclinical AD is an essential research focus as it is seen as the most promising model for developing therapies to modify the disease (Hampel & Broich, 2009).

A preclinical rat model of AD was used in the current study to examine how pretangle tau in the LC affects astrocytic glycogen metabolism in the hippocampus. Researchers at Memorial University of Newfoundland created this rat model to replicate Braak's pretangle staging of AD. The approach required inserting the human pseudophosphorylated tau (htau) gene into the LC. According to Ghosh et al. (2019), pseudophosphorylation was utilized to simulate the effects of persistently phosphorylated tau. The LCs of rats received bilateral injections of adeno-associated viral (AAV) vectors containing the transgene for pseudophosphorylated human tau (htauE14) protein. This pseudophosphorylated htau model was shown by Ghosh et al. (2019) to properly depict the progression of abnormal tau found in Braak's pretangle stages. The infusion of htauE14 in the LC initiated the development of soluble hyperphosphorylated pretangle stages in tyrosine hydroxylase (TH)-Cre rats (Ghosh et al. 2019).

The current study aimed to examine metabolic changes in glycogen, specifically by assessing the activity of GP. This enzyme breaks down glycogen for neuronal metabolism in different stages of AD in the hippocampus. Additionally, the study investigated the astrocytic GFAP profile in both male and female rats' dentate gyrus, CA1, and CA3 regions. Animals in the htauE14 group, who received bilateral infusions of a virus containing the gene for pseudophosphorylated htau in the LC, were compared to animals in the control group, which either got infusions of the same virus without the gene, vehicle infusions or were left unoperated. It was hypothesized that LC-htauE14 infused animals would have higher hippocampal GP activity and astrocyte reactivity compared to control animals. It was also hypothesized that htauE14 female rats would exhibit increased levels of GP and corresponding altered GFAP pattern compared to male rats.

2. Materials and Methods

2.1 Subjects

The study protocol and the treatment of animals in the research adhered to the guidelines specified by the Canadian Council of Animal Care and approved by the Institutional Animal Care Committee of Memorial University (Animal Utilization Protocol 18-02-SW).

The experiment involved both male (n = 10) and female (n = 10) transgenic TH-Cre$^{+/-}$ Sprague-Dawley rats as they enabled specific expression of htauE14 in the LC neurons. The housing for the animals involved one rat per cage, and in addition, the animals were provided with a 12-hour cycle of light and darkness (lights on 1900 h). The cages were placed in a colony room where the temperature was regulated at 20^{o}C. The rats were individually kept and put on a

restricted food intake after the infusion process. They received 75% of their average daily food amount to retain a healthy weight but had access to unlimited water.

2.2 Experimental Design and AAV LC Infusion

At the age of 3 months, rats in the experimental group (n = 10) were administered two infusions of AAV2/9-rEF1a-DIO-EGFP-htauE14-WPRE, 2.05E+13vg/mL (Virovek), referred to as "LC-htauE14". These infusions were administered directly into each hemisphere. In contrast, the control animals (n = 10) either received injections of a similar virus that did not contain the htauE14 transgene (AAV2/9-EF1a-FLEX- EGFP; 1.8E+13vg/mL; Laval Neurophotonics, QC), a sham operation but no infusion, or were left unoperated. The infused control animals received two 0.5 µl of the viral vector in each hemisphere.

Isoflurane anesthesia (2-5%) was used for all surgical procedures. Subsequently, the animals were positioned in a stereotaxic device in a flat skull position, and body temperature was regulated at 37°C. They were then administered an analgesic (Meloxicam SR, at 4mg/kg, 10mg/mL, s.c.) A scalp incision was made, and on each side of the sagittal suture, a single hole was drilled using bregma as a reference point. The coordinates for these drill sites were approximately 12.2 mm posterior to bregma along the anterior-posterior axis and ±1.3mm lateral from the mid-line along the medial-lateral axis. Cannulas were inserted into these drill sites at a 20° angle posterior to the vertical axis, reaching a depth of about 6.4mm below the brain's surface. The infusions into the LC were carried out using autoanalyzer tubing (Fisher) and a 5 µl microsyringe (Hamilton) at a rate of approximately 1.0 µl/min.

The post-op monitoring process was initiated and continued until suture removal. This monitoring included daily assessments and documentation of the animals' weight and incision sites to ensure the animals' continued good health and prevent major complications. In the 14–23-month period following LC infusion, animals were euthanized for histology and immunohistochemistry. The experiment consisted of AAV-htauE14-GFP (n = 10) and controls (n = 10); sham (n = 3), vehicle (n = 3), and AAV-GFP (n = 4). A total of 20 rats were used in the study, with an equal number of male and female rats.

2.3 Preparation of Brain Tissue

All animals were euthanized during the dark phase (red light) of the light cycle. Tissue extraction occurred at ~20 months post-infusion. Rats were anesthetized via inhalation of isoflurane induced at 1% concentration, increasing to 3.5% for females and 4% for males over one minute for rapid induction. This level was maintained for an additional 5-6 minutes until a negative toe-pinch test confirmed the appropriate anesthetic depth. Subsequently, the rats were taken out of the induction chamber and euthanized by guillotine decapitation.

Tissue extraction was also performed in a dark environment under red light (to avoid disruptions in the animals' circadian rhythm) at the average age of 19.8 months (SD = 4.40) for male rats and 19.9 months (SD = 3.08) for female rats post-infusion (p.i). All the brains were frozen in methyl-butane cooled to -70°C and stored at -80°C. Attempts were made to keep the average time from decapitation and brain extraction to flash frozen constant across conditions. The average time from decapitation to freezing for male rats was 2 minutes and 49 seconds (SD= 0.212) and 2 minutes 43 seconds (SD = 0.0314) for females. Sections from one hemisphere of htauE14 rats were matched with sections from control rats. These sections were then frozen simultaneously for the same amount of time and subjected to concurrent treatment.

2.4 Glycogen Phosphorylase Histochemistry

The current study used previously published GP histochemical procedures (Walling et al., 2006; Walling et al., 2007; and Meijer, 1968). In summary, I performed a chimeric mounting of rats' brains by which brains were sectioned in the horizontal plane, and hemispheres were matched between the LC-htauE14 (experimental) and LC-control animals. This allowed for concurrent tissue processing in the histochemical and immunohistochemical conditions. A Cryostat was used to slice fresh frozen tissue into 30 μm sections, creating four types of slides (Nissl, aGP, tGP, and 'Extra') and preserved in a -80 ^{o}C freezer until further processing.

To measure aGP, sections were incubated for 30 minutes at 37 °C in α-D-glucose-1-phosphate (1.6g), EDTA (0.4g), NaF (0.32g), and dextran (8.0g; 30,000-40,000 MW) dissolved in 40 mL of sodium acetate buffer (pH 5.6) and to 200 mL with distilled water (pH 6.0) (Walling et al., 2007). The incubation medium for assessing tGP activity involved the steps outlined above for aGP and also included adenosine 5′- mono-phosphate (0.16g) (Walling et al., 2007). Sections were allowed to air-dry (20–25 minutes), fixed in 40% ethanol for 4 minutes, air-dried again for 15–20 minutes, and finally dipped in Lugol's iodine solution (consisting of 11% sucrose) for approximately 3 minutes. After air-drying overnight, the sections were covered with Permount (Fisher Scientific, Waltham, MA) and kept in a dark space until further processing.

2.5 Imaging and Relative Optical Density (ROD) Measurements of aGP and tGP

A Brightfield light microscope (Olympus BX52) and a DP90 camera were used to capture brightfield images at 4x magnification. Colored images were converted to grayscale using Irfanview (version 4.60) and densitometrically analyzed using MCID analysis software (Interfocus

Ltd; Linton, UK, version 7.1). The DG, CA3 and CA1 (15 subsections) of the hippocampus were the areas included in the relative optical density analyses (see Figure 2). Ventral and dorsal sections (2 each) were selected from each pair of animals for analyses. The gray levels of DG, CA3 and CA1 were derived by calculating the average of 10 measurements from individual sections for each animal. Sections measured for optical density in each of the hippocampal regions were subjected to graphical and statistical analysis.

Label of the subregions of the hippocampus (DG, CA3 and CA1) and the hippocampal synaptic circuit

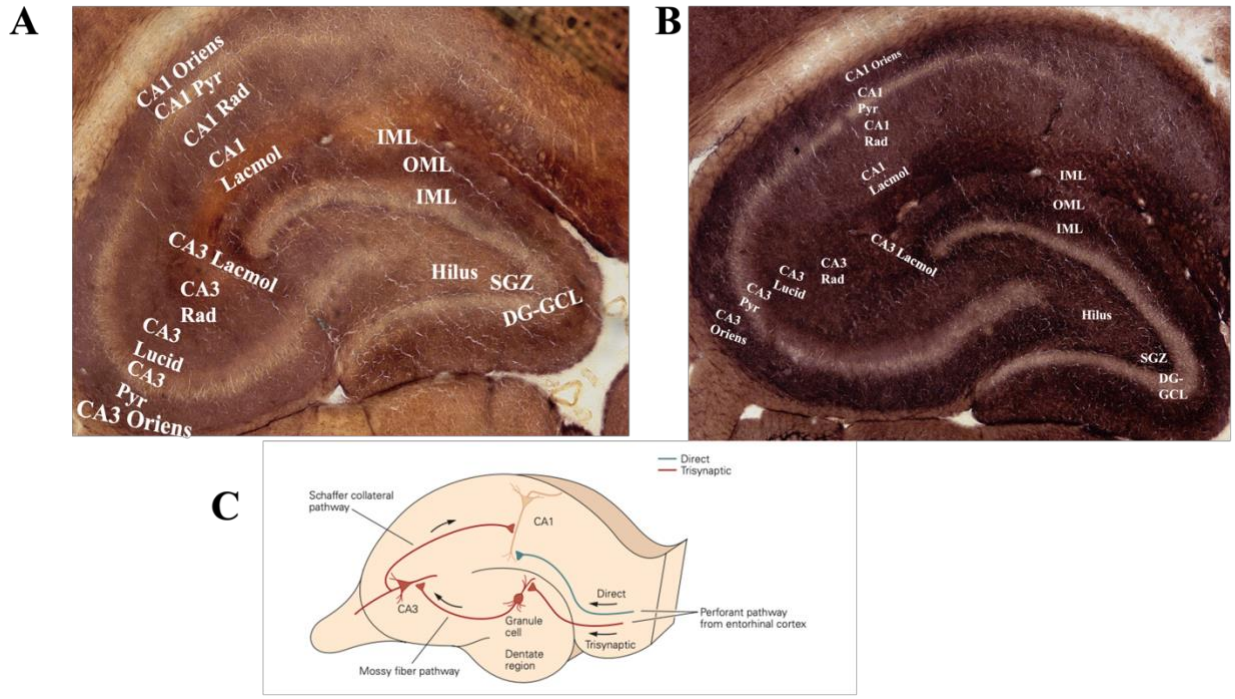

Figure 2. **A and B:** Brightfield images of active glycogen phosphorylase (aGP) and total (tGP) histochemistry in the hippocampus of a rat at 4x magnification. The label shows 3 major regions of the hippocampus that were investigated: cornu ammonis 1 (CA1), cornu ammonis 3 (CA3) and dentate gyrus (DG) (Lethbridge et al., 2014). The four subregions of the CA1 include: CA1 lacunosum moleculae (CA1 lacmol), CA1 oriens, CA1 pyramidal cells (CA1 pyr), and CA1 radiatum (CA1 rad). For the CA3, the five subregions include CA3 lacunosum moleculare (CA3 lacmol), CA3 lucidum (CA3 lucid), CA3 oriens, CA3 pyramidal (CA3 pyr), and CA3 radiatum (CA3 rad). Dentate gyrus had six subregions: Dentate gyrus-granular cell layer (DG-GCL), hilus, inner molecular layer (IML), middle molecular layer (MML), outer molecular layer, and subgranular zone (SGZ).

C: The synaptic circuitry within the hippocampus is crucial in declarative memory (Image adapted from Kandel et al., 2014). Information flows into the hippocampus from the entorhinal cortex via perforant pathways, providing direct and indirect input to CA1 pyramidal neurons, which are essential hippocampal output cells. Entorhinal cortex layer II neurons project through the perforant path to stimulate granule cells in the DG in the indirect pathway. Granule cells activate pyramidal cells in CA3 via the mossy fiber pathway, which then excites CA1 pyramidal cells through the Schaffer collateral pathway. Layer III neurons from the entorhinal cortex project directly through the perforant path to activate the distal dendrites of CA1 pyramidal neurons, with no intermediary synapses in the direct pathway.

2.6 Immunohistochemistry and GFAP Astrocyte Analysis

Immunohistochemical processing on fresh frozen tissue was performed by first washing the sections in Tris buffer for 3x5 min. Sections were then treated in 1% hydrogen peroxide (1ml of 30% hydrogen peroxide to 29ml of Tris buffer) for 30 min. Sections were washed in Tris buffer, Tris A and Tris B for 5 and 10 min, respectively. This was followed by incubating slides in 10% normal horse serum (Vector Labs) made in Tris B for an hour (to ensure the binding of nonspecific antigens). Slides were washed in Tris A and B for 10 min each. Sections were then incubated in appropriate dilution and volume of primary mouse antibody (mouse, Millipore) made in Tris B except for the no-antibody control (NAB) overnight on a rotator. The NAB was incubated in Tris B for the same duration.

Sections were washed in Tris A and B for 10 minutes the next day and incubated in biotinylated horse anti-mouse IgG (Vector Labs) at 1:400 (5ml + 2ml Tris B) concentration for 1 hour at room temperature on a rotator. Slides were washed in Tris A and D for 10 min each and incubated in ABC Elite 1:1000 (5µl + 5µl) to 5ml Tris D for 90 min. Slides were washed in Tris buffer for 3x5 min.

The sections were incubated in DAB (diaminobenzidine tetrahydrochloride; Metal Enhanced DAB substrate kit; ThermoFisher) solution (consisting of 10% DAB and 90% DAB buffer) from Polysciences for 15-30 min. Sections were removed from DAB solution when staining is deemed to be optimal and washed in Tris buffer for 3 x 5 min. Sections were then air-dried overnight. Sections were dehydrated with ethanol and xylene and coverslipped with Permount for further processing. The protocol for dehydration involved washing slides in 70%

ethanol (2-3 min), 95% ethanol (2-3 min), 100% ethanol (2-3 min, 2 changes) and xylene (2-3 min, 2 changes).

For astrocyte analysis, brightfield images were captured using a microscope and camera (described in the previous section for GP). Brightfield Images were analyzed using Fiji ImageJ software (version 1.53y; Maryland, USA). After converting images to grayscale, a Kodak Step Tablet (No. 705ST801) was used to calibrate images to a densitometric standard and manually drawn region of interest (oval w = 0.75 [74], h = 0.75 [74]). Astrocyte profile density of the various subregions of CA1, CA3 and DG were determined by averaging five measurements of four sections from each animal and subtracting its corresponding NAB values.

2.7 Statistical Analyses and Graphical Presentation.

Jamovi version 2.4.8.0 (Sydney, Australia) was used to conduct all statistical analyses. The statistical analyses were performed on matched samples (htau versus control). I conducted a repeated measures ANOVA (as used in a similar study by Walling et al., 2007) comparing sex, condition and subregion for aGP, tGP, ratio and GFAP astrocytes. For the post-hoc analysis of the ANOVA data, Tukey's HSD post hoc test was utilized to evaluate comparisons between pairs, and a significance level of $p < .05$ was used to determine the statistical significance between the pairs.

Prism version 9.4.0 (Boston, USA) was used to plot graphs of GP and astrocyte activities in the various regions of the hippocampus. This was to aid in visual interpretation of the effects of sex and condition in the DG, CA3 and CA1 areas.

3. Results

3.1 Introduction

The present study investigated astrocytic glycogen by averaging the GP and astrocyte ROD measurements within the hippocampal structures (DG, CA3, and CA1) at ~20 months p.i. ROD measurements of GP and astrocytic GFAP profile of rats in the experimental group (LC-htauE14 infused) were compared with control animals. Also, sex-specific differences were considered. The results of aGP, tGP, ratio data and astrocyte GFAP pattern in the DG, CA3 and CA1 are presented below.

3.2 Phase 1: Glycogen Phosphorylase Activity in Rat Hippocampus ~20 months post LC-htauE14 infusion

3.2.1 The Dentate Gyrus

The DG of the hippocampus is made up of highly packed granule cells and a layer of long-projecting neurons in the hilus (Acsády et al., 1998). Granule cells obtain input from the entorhinal cortex and transmit excitatory signals to the CA3 subfield through mossy fibres (Acsády et al., 1998) (see Figure 2C). This highlights the DG's significance in memory encoding, particularly for episodic and spatial memories (Barbosa et al., 2012).

aGP activity in the DG ~20 months p.i

The "active" form of GP (aGP) refers to the functional and catalytically prepared state of the enzyme (Cori & Cori, 1945). In its active state, GP can efficiently cleave glucose units from

glycogen, initiating the conversion of glycogen into glucose-1-phosphate for energy production (Cori & Cori, 1945; Fischer & Krebs, 1955).

A 3-way repeated measures analysis (sex x subregion x condition) revealed no significant effect of LC-htauE14 infusion on aGP relative level in the DG. Moreover, the ROD measurement of aGP activity in the DG revealed no condition-dependent (condition x subregion) interaction. However, a significant subregion x sex interaction ($F_{5, 80} = 3.346$, $p = .009$) was found within the DG. Tukey's HSD post-hoc analyses of GP ROD measurements did not reveal any sex-dependent differences between male and female rats in the various subregions of the DG (see Figure 3A). Analysis of the ROD measures revealed a significant main effect ($F_{5,80} = 122$, $p < .001$) in the various subregions of DG. Tukey HSD post-hoc test found that the MML (0.526) had the highest level of aGP activity, followed by the SGZ (0.481) and OML (0.420). The DG-GCL had the lowest level of aGP activity (0.257), followed by the IML (0.368) and Hilus (0.375).

The overall results revealed that at ~20 months p.i, LC-htauE14 infusion did not alter aGP relative level in the hippocampal DG. No significant sex differences were found. However, the MML, SGZ and OML were the DG subregions with the highest aGP activity, while the DG-GCL and IML recorded the lowest level of aGP (see Figure 3A).

tGP activity in the DG ~20 months p.i

The term "total" in GP (tGP) denotes the entire quantity of the enzyme, which includes both active and inactive forms, providing a full picture of the enzymatic capability for glycogen breakdown. Similar to the aGP results, no 3-way (sex x subregion x condition) and condition-dependent (condition x subregion) interactions were observed for tGP activity in the DG. A

significant sex x subregion ($F_{5, 80} = 3.063$, $p = 0.014$) interaction was observed. However, Tukey HSD post-hoc revealed no sex-dependent differences between male and female rats. A significant main effect ($F_{5,80} = 148$, $p < .001$) was observed in the subregions of the DG (see Figure 3B). The Tukey post-hoc analysis showed that the highest GP ROD measurements were found in the MML (0.858), SGZ (0.824) and the OML (0.717). The lowest tGP levels were recorded in the DG-GCL (0.384), IML (0.633) and Hilus (0.712).

Ratio GP (aGP:tGP) in the DG

The ratio GP signifies the percentage of active enzyme relative to the total enzyme present. It shows the readiness for glycogen breakdown to produce energy when required. Higher ratios imply increased enzymatic activity, which may indicate an increase in glucose synthesis and glycogenolysis.

Similar to results reported in the aGP and tGP activity in DG, there was no significant 3-way (sex x subregion x condition) and 2-way interaction (condition x subregion) in the ratio analyses. Interestingly, no significant sex-dependent effect (sex x subregion) was also detected. However, a significant main effect ($F_{5,80} = 19.8$, $p < .001$) of ratio GP activity was observed in the DG subregions (see Figure 3C). Contrary to the findings from aGP and tGP levels, the Tukey post-hoc analysis revealed that the DG-GCL had the highest ratio (0.676) of GP ROD measurement, followed by the MML (0.621) and the IML (0.602). The hilus had the lowest ratio of GP activity (0.531), followed by the SGZ (0.589) and the OML (0.592).

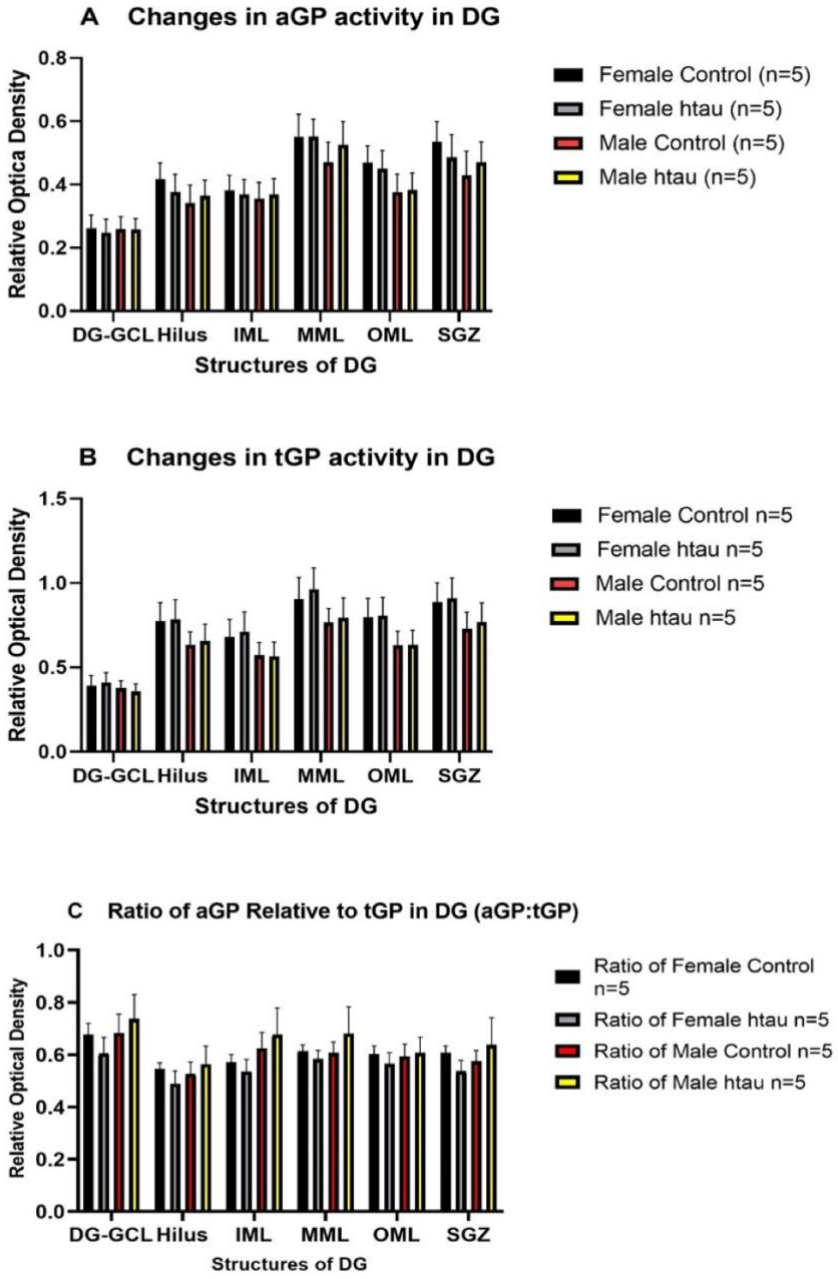

Figure 3: Graph **A-C** shows the relative optical density (ROD) of aGP, tGP and ratio activity for htauE14 animals and controls as well as sexes (males and females) at ~20 months p.i in the DG. Graph **A** depicts data for aGP activity, graph **B** shows tGP activity in the various subregions of the DG, and **C** depicts the ratio GP activity in the DG. All data are represented by means (+ SEM), *n* = 20

3.2.2 The Hippocampal CA3

CA3 is a crucial region within the hippocampus. It is heavily populated with pyramidal neurons and is important for consolidating and retrieving memories (Nakashiba et al., 2009), especially those related to spatial and episodic memory (Barbosa et al., 2012).

aGP activity in the CA3 subfield of the Hippocampus ~20 months p.i

The aGP repeated measures analyses revealed no significant 3-way interaction in the CA3. The 2-way analysis (subregion x condition) revealed no significant interaction in aGP ROD measurements between the treatment condition (htauE14) and control in the CA3 subregions. However, I found a significant interaction (subregion x sex) in the CA3 ($F_{4, 64}$ = 4.291, p = .004), with no specific sex-dependent effect from the Tukey post-hoc. A significant main effect was observed among the CA3 subregions ($F_{4, 64}$ = 102.8, p < .001). The Tukey follow-up comparisons indicated that the CA3 lacmol (0.423) had the highest aGP activity, followed by oriens (0.395) and the CA3 rad (0.363). The CA3 pyr (0.229) and the CA3 lucid (0.289) had the lowest level of GP ROD measurements in the hippocampal CA3 (see Figure 4A).

tGP activity in the CA3 subfield of the Hippocampus ~20 months p.i

The GP ROD measurement of tGP activity in the CA3 is similar to what was reported above for the aGP in the 3-way and 2-way (subregion x condition) and (subregion x sex) interactions. Similar to aGP, a main effect was revealed among the subregions of the CA3 ($F_{4, 64}$ = 104.657, p < .001). The post-hoc showed the same trend (as reported for aGP above) regarding regions with the highest and lowest tGP ROD levels in the CA3 subregions (see Figure 4B).

Ratio activity in the CA3 subfield of the Hippocampus ~20 months p.i

Ratio GP analysis of GP ROD measurement showed no significant 3-way interaction effect and no 2-way (sex and condition) interaction in the CA3. However, there was a significant main effect within the subregions ($F_{4, 64} = 8.489$, $p < .001$). Means ranked from the post hoc analysis revealed the pyr (0.562) as having the highest GP ratio activity, followed by the lacmol (0.554) and the lucid (0.526). On the other hand, the lowest level of ratio activity within the CA3 was found in the oriens (0.501) and rad (0.518), as shown in Figure 4C.

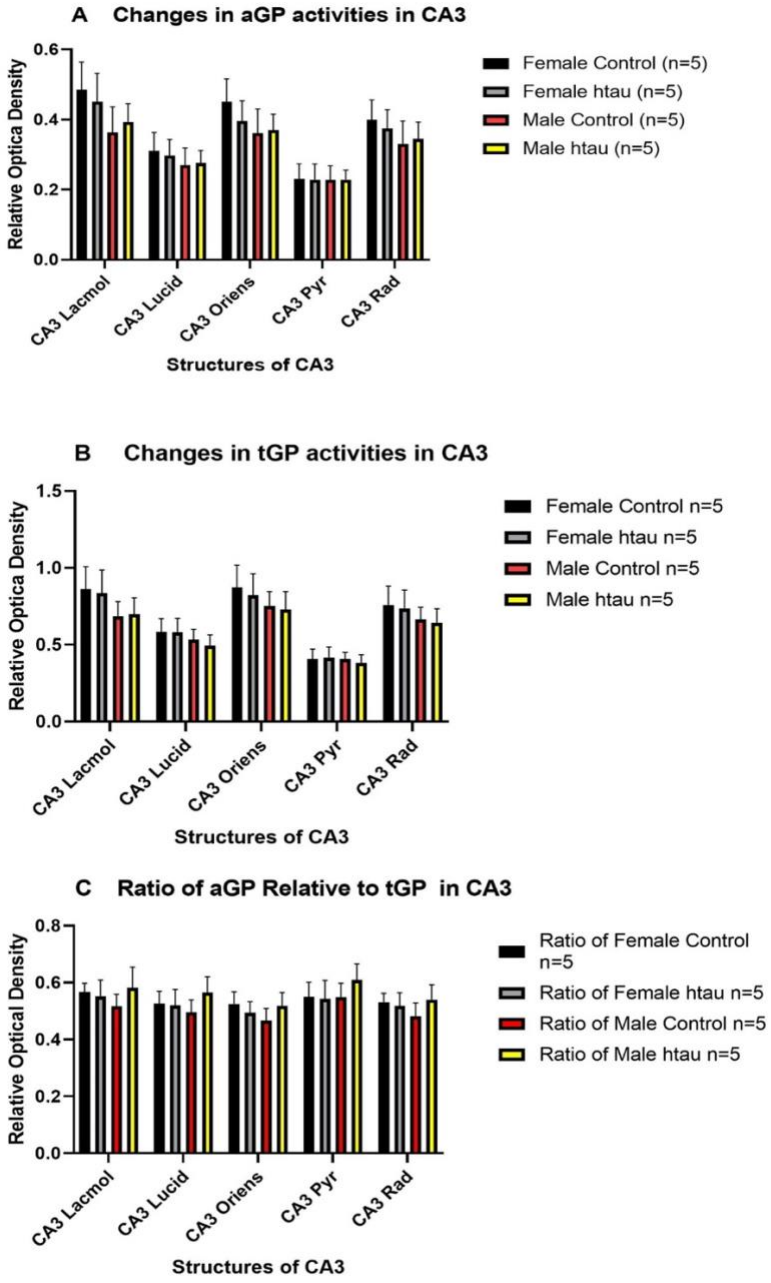

Figure 4: Graph **A-C** highlights the ROD measurements of aGP, tGP and ratio activity for htauE14 animals and control as well as sexes (males and females) at ~20 months p.i) in the CA3. Graph **A** depicts data for aGP activity, graph **B** shows tGP activity in the various subregions of the CA3, and **C** depicts the ratio of GP activity in the CA3. All data are represented by means (+ SEM), *n* = 20

3.2.3 The Hippocampal CA1

CA1 is a significant area of the hippocampus predominantly made of pyramidal neurons. The CA1 integrates and processes the information received from the CA3 subfield (Schlichting et al., 2014) (see Figure 2B). It combines input from both the Schaffer collaterals (axons originating from CA3 neurons) and the perforant path (entorhinal cortex fibres). This integration process aids in memory consolidation and encoding of contextual and spatial memories (Schlichting et al., 2014). CA1 is the main output area of the hippocampus (Delatour & Witter, 2002). It plays a significant role in transferring processed information to other regions in the brain (Delatour & Witter, 2002).

aGP activity in the CA1

The result from the 3-way repeated measures analysis (subregion x Sex x Condition) on GP ROD Measurements showed no significance. Also, the 2-way analysis (subregion x condition) revealed no significant interaction in aGP ROD measurements between the treatment condition (htauE14) and control in the CA1 subregions. However, despite finding a significant sex-dependent interaction in CA1 (subregion x sex) $F_{3, 48} = 3.887$, $p = .014$, the Tukey post-hoc analysis revealed no differences between females and males. I observed a significant main effect (subregions) within the CA1 ($p < .001$). The CA1 lacmol (0.374) had the highest level of aGP activity, followed by the oriens (0.336) and the CA1 rad. The CA1 pyr (0.199) recorded the lowest level of aGP activity within the CA1 subregions (see Figure 5A).

tGP activity in the CA1

Similar to the findings reported above, there were no significant 3-way interactions or condition-dependent interactions. A significant 2-way interaction (subregion x sex) was found

within the CA1 ($F_{3, 48} = 2.936$, $p = .043$), with no sex-dependent differences from the post-hoc analysis. The main effect found within the subregions is identical to what was reported for the aGP ranked from highest to lowest (CA1 Lacmol, oriens, CA1 rad and CA1 pyr) (see figure 5B).

Ratio activity in the CA1

I further investigated whether the amount of total GP expressed in the active form (breakdown of glycogen) changes in relation to conditions of LC-htauE14 infusion or sex in ~20 months p.i rats. This ratio helps to normalize the data and account for any differences in the amount of tGP in the hippocampus, which could influence the measurement of GP activity.

There were no significant 3-way, condition, or sex-dependent interactions in GP ratio within the CA1 region. However, a significant main effect was found within the CA1 subregions of the hippocampus ($F_{3, 48} = 10.839$, $p < .001$). Contrary to what was found in the aGP and tGP measurements, the Tukey post-hoc analysis revealed the CA1 pyr (0.560) as the subregion with the highest ratio activity, followed by the CA1 rad (0.554). The oriens (0.497) and lacmol (0.515) had the lowest ratio activity within the CA1 (see Figure 5C).

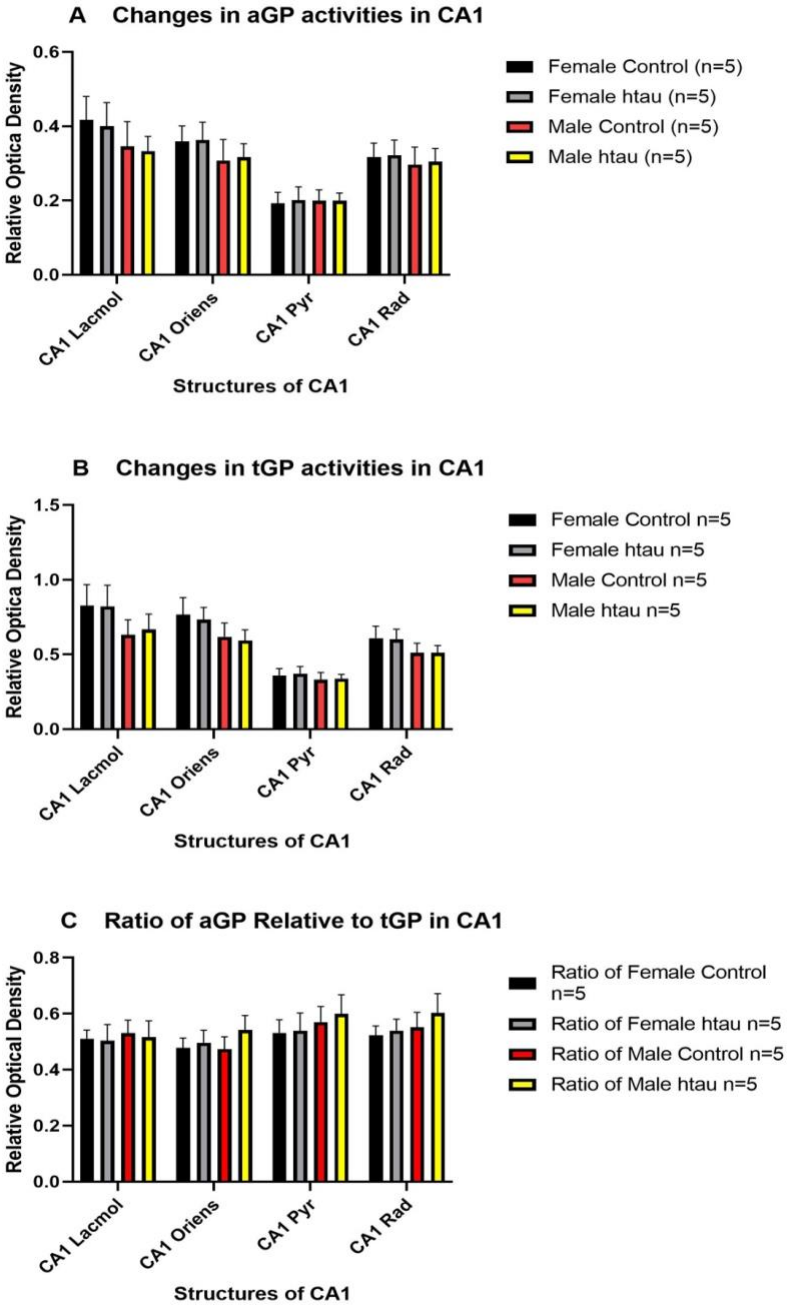

Figure 5: Graph **A-C** shows the ROD of aGP, tGP and ratio activity in the CA1. Graph **A** depicts data for aGP activity, graph **B** shows tGP activity in the various subregions of the CA1, and **C** depicts the ratio GP activity of the various subregions within the CA1. All data are represented by means (+ SEM), *n* = 20

3.3 Phase 2: Astrocytic (GFAP) Profile in the Hippocampus of Rats ~20 Months Post-LC-htauE14 Infusion.

Astrocytes, identified by the protein marker GFAP, are abundantly present in the hippocampus and its subregions (DG, CA3 and CA1). Astrocytes are known to contain GP, which is responsible for the breakdown of glycogen into metabolic substrates to be used by neurons and astrocytes (Swanson et al., 1992). I examined astrocyte expression in a pretangle model of AD (see Figure 6) to see if any changes in GFAP expression would translate to changes in GP activity in older rats (~20 month p.i).

Similar to findings from the GP analyses, the 3-way analysis revealed no significant interaction within the hippocampus's DG, CA3 and CA1 regions. I then conducted 2-way analyses to determine whether any differential astrocytic profile exists among the groups. No significant 2-way interaction (condition-dependent) in all the regions and no significant sex-dependent interaction (sex x subregion) were found in the CA3 and CA1 subregions. However, in the DG, subregion x sex analysis was significant ($F_{5, 80} = 2.467$, $p = .03$) with no sex-specific differences from the Tukey HSD post-hoc analysis (see Figure 7).

I then investigated potential differences within the various subfields of the hippocampus. A significant main effect ($F_{5, 80} = 73.8$, $p < .001$) in the DG, CA3 ($F_{4, 64} = 72.48$, $p < .001$) and CA1 ($F_{3, 48} = 121.073$, $p < .001$) subregions were found (see Figure 6A-6C). In the Tukey HSD post-hoc analyses, the subregions of each hippocampal subfield were ranked to determine subregions with high or low astrocytic density. In the DG, the MML (0.039) had the highest level of astrocyte GFAP, followed by the IML (0.03) and the Hilus (0.029). The OML, on the other hand, had the lowest level of astrocytic expression (0.019), followed by DG-GCL (0.02)

and then SGZ (0.026). Within the CA3 region, subregions with high GFAP astrocytic profiles were CA3 oriens (0.035) and CA3 lucid (0.021. In contrast, the CA3 pyr (0.013), CA3 lacmol (0.015) and CA3 rad (0.016) had lower astrocytic GFAP activity. Lastly, the CA1 oriens (0.039) and CA1 lacmol had high levels of GFAP density, while the CA1 rad (0.015) and CA1 pyr (0.022) recorded lower levels of GFAP pattern (see Figure 7).

The overall results from the GFAP analyses highlight no significant effect of LC-htauE14 infusion on the astrocytic profile of older rats (~20 months p.i). No noticeable difference between male and female rats' astrocyte profiles was observed. Areas such as MML and Hilus of the DG, oriens and lucid of the CA3 region, and oriens and lacmol of the CA1subfield showed high levels of astrocyte ROD measurements. Within the DG, the OML, DG-GCL and SGZ are areas with reduced astrocytes. In the CA3 and CA1, the pyr, rad and lacmol are areas with low levels of astrocytes.

Brightfield images of the astrocyte marker GFAP in rat hippocampus

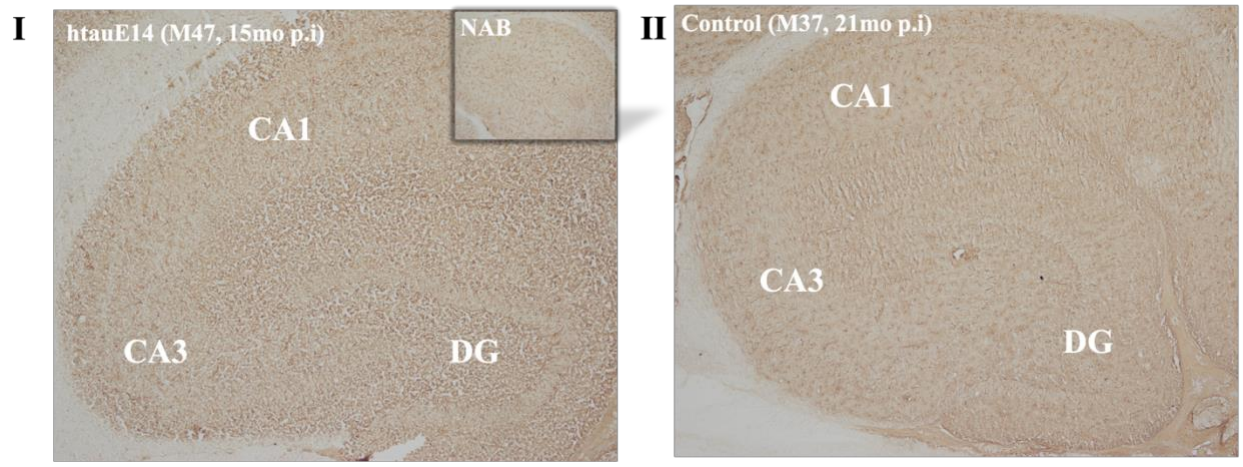

Figure 6: Brightfield images of GFAP profile in the hippocampal DG, CA3 and CA1 of a rat at 4x magnification for **(I)** htauE14 (15mo, pi) and **(II)** control (21mo, pi) animals. *Inserted image:* Tissue slice that did not undergo primary antibody treatment. NAB = No antibody.

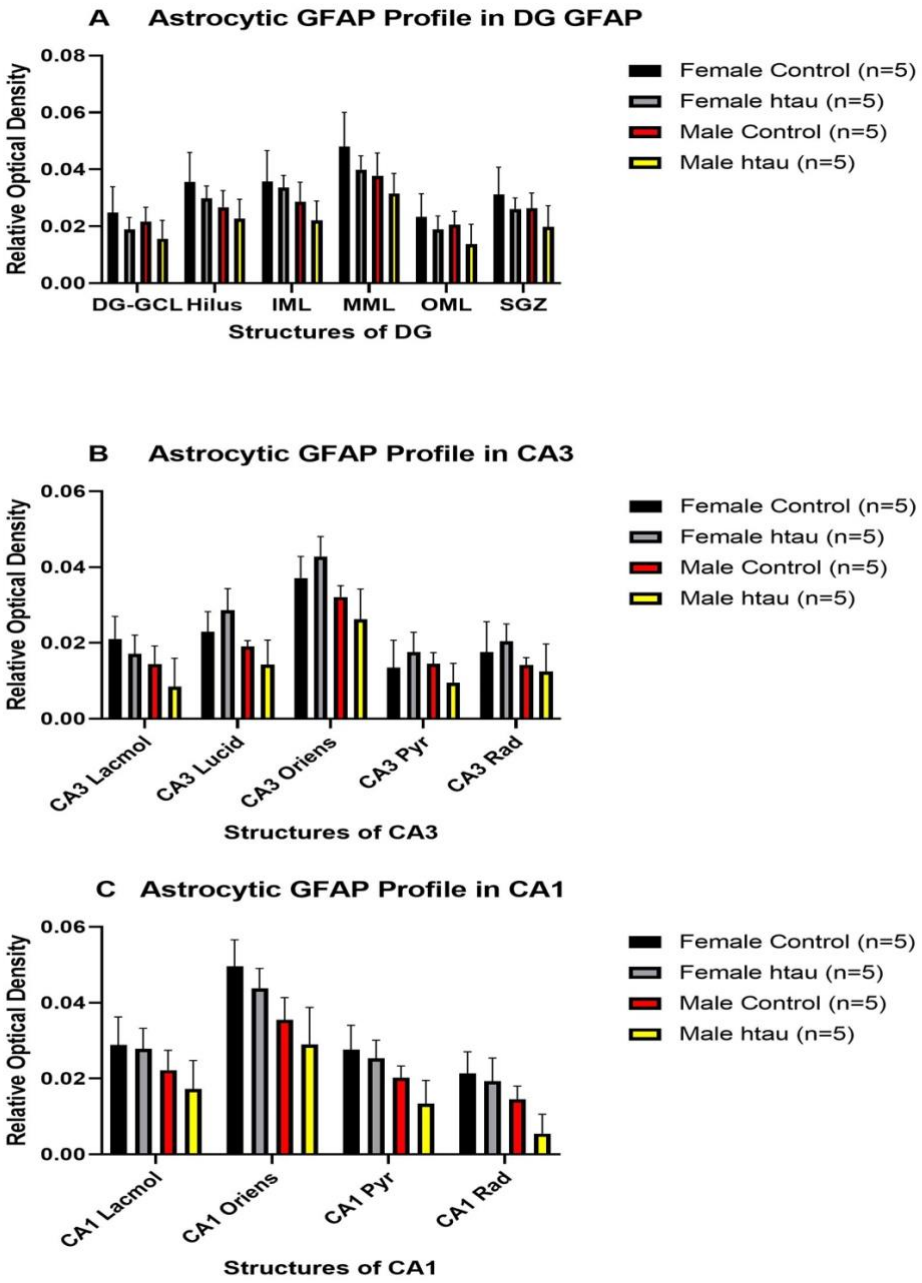

Figure 7: Graph **A-C** represents the ROD) of astrocytic GFAP profile for htauE14 animals and control as well as sexes (males and females) at ~20 months p.i) in the DG, CA3 and CA1 of the hippocampus. Graph **A** depicts data for the GFAP pattern in the DG, **B** shows astrocyte ROD measurement in the various subregions of the CA3, and **C** depicts the astrocyte GFAP expression in the CA1. All data are represented by means (+ SEM), *n* = 20

4. Discussion

4.1 Summary of Major Findings

The present study explored whether the insertion of htauE14 into the LC of heterozygous TH:Cre male and female rats affects the GP relative levels and astrocyte expression within the hippocampal structures (DG, CA3, and CA1) at ~20 months p.i.. ROD measurements of GP and astrocytic GFAP profile of rats in the experimental group (LC-htauE14 infused) were compared with control animals. Additionally, sex-specific variations were considered. The experiments were carried out in two phases. In phase 1, I investigated the various GP relative levels (aGP, tGP and ratio) in the subfields (DG, CA3 and CA1) of the hippocampus by averaging the ROD measurements of their various subregions. LC-htauE14 infusion did not alter the GP levels (aGP, tGP, and ratio) in the DG, CA3 and CA1 in these older rats (~20 months p.i), and no sex-dependent alterations were detected. Distinct regional variations in GP activity were observed within the hippocampal subfields. Higher levels of aGP and tGP were found in specific areas of DG, CA3 and CA1. Additionally, the GP ratio varied across different brain regions.

In phase 2, I probed into the expression of GFAP in the DG, CA3 and CA1 subfields of the hippocampus to ascertain whether the astrocytic ROD levels are commensurate with the GP ROD levels found in these older rats at the pretangle stage of AD. Similar to findings from the GP analyses, LC-htauE14 infusion did not alter the GFAP profile in the hippocampus of older rats (~20 months p.i) at the pretangle stage of AD. Some regions of the DG, CA3 and CA1 exhibited elevated levels of astrocyte ROD, while lower levels were observed in areas like OML DG-GCL. Together, these results suggest that LC-htauE14 infusion did not affect the relative levels of GP and astrocytic GFAP expression within the hippocampus of older rats (~20 months

p.i) at the early stages of AD pathology. The findings also suggest that various subregions within the hippocampal DG, CA3 and CA1 showed different levels of GP and GFAP profiles regardless of sex and condition.

4.2 No Effect of LC-htauE14 on ROD of GP (aGP, tGP or ratio)

4.2.1 LC-htauE14 did not alter the ROD of aGP, tGP or ratio measures in older rats at the pretangle stage of AD

One of the major hypotheses of the current study was that LC-htauE14 would affect the ROD of aGP, tGP and ratio measures in the hippocampal DG, CA3 and CA1 at the pretangle stage. However, this hypothesis was not supported; LC-htauE14 did not alter the ROD of GP. This result was not predicted as previous studies on AD have reported a relationship between changes in glycogen metabolism and AD (Mann et al., 1987; Plaschke & Hoyer, 1993).

In a study on humans, Mann et al. (1987) reported an accumulation of glycogen in the cerebral cortex of AD patients. Mann et al. (1987) asserted that the accumulation of glycogen in the cerebral cortex during AD may be linked to disturbed axonal transport resulting from senile plaques. Moreover, in animal studies, Plaschke and Hoyer (1993) administered an intracerebroventricular (icv) injection of streptozotocin (STZ), a drug that inhibits insulin, into rats and examined its effects on energy metabolism within the hippocampus and cerebral cortex. This method induced conditions resembling aspects of AD in these rats through the inhibition of insulin release and decrease in insulin receptor signaling with the resultant occurrence of diabetes mellitus. The study reported a significantly higher glycogen content within the hippocampus of STZ-treated rats relative to controls (7% in 3 weeks and 15% in 6 weeks). They found decreased aGP enzymatic activity within the hippocampus. Particularly, there was a 30%

reduction in aGP activity at 3 weeks and 15% decrease in 6 weeks post STZ injection (Plaschke & Hoyer, 1993).

As these studies found changes in glycogen content and aGP activity in AD, it was predicted that these changes would be translated into the relative activity of GP at the pretangle stage of AD. A possible explanation of the findings from the present study is that changes in GP activity may be subtle in the pretangle stage of AD until the appearance of AD-related symptoms, or there may be compensatory mechanisms such as the upregulation of beta-1 adrenoceptors that may account for energy deficits at the pretangle stage (Ghosh et al., 2019; Szot et al., 2006; Szot et al., 2007). Additionally, I hypothesize that duration following htau infusion could also be a potential factor that might contribute to compensatory processes. Do GP levels and astrocyte reactivity remain the same in older infused rats at varying durations post-infusion, and does this period provide an avenue for compensatory activities to occur? Perhaps GP differences would be found in other brain regions, closer to the infusion sites? These questions warrant further investigation in subsequent studies.

Comparison to the ANLS Model

Contrary to the ANLS hypothesis, the present study found no effect of LC-htauE14 on GP ROD in older rats (20 months post infusion). The ANLS model suggests that glucose is primarily utilized by astrocytes, converted to lactate, and subsequently used by neurons for energy production (Pellerin & Magistretti, 1994). Previous studies supporting the ANLS showed inhibition of glycogen breakdown and lactate release from astrocytes impacting memory consolidation (Gibbs et al., 2006) and Long-Term Potentiation (LTP) (Suzuki et al., 2011). However, all these studies used younger animals (Gibbs et al., 2006; Suzuki, 2011). In contrast to the ANLS theory, Drulis-Fajdasz et al. (2018) discovered that unlike results from younger

animals which supported the ANLS theory, their investigation on older mice showed increased levels of glycolytic enzymes such as GP in neurons. Hippocampal neurons of older mice did not depend on lactate generated from astrocytes questioning the existence of the ANLS in older animals. This result is consistent with the findings from my current investigation and may help to explain why the effects of LC-htauE14 on GP ROD were absent in older rats. Nonetheless, further research, including analysis of GP ROD in younger animals at the pretangle stage of AD (currently ongoing in our lab), is needed for a more conclusive understanding of changes in GP ROD throughout the lifespan and under AD condition.

4.2.2 LC-NE System and AD Pathology

The present study revealed that LC-htaE14 did not alter the GP ROD within the hippocampal DG, CA3 and CA1 at the pretangle stage in older rats. Numerous studies on both humans and animals have long noted the changes in the noradrenergic system associated with AD (Ghosh et al., 2019; Mann et al., 1980; Matthews et al., 2002; Omoluabi et al., 2021). This phenomenon has been well described in animals, yet not enough research has been done to determine how it affects AD pathogenesis. Ghosh et al. (2019) highlighted significant LC cell loss and decreased NET fiber density within the piriform cortex and hippocampus of older htauE14-infused rats (14-16 months old) at the pretangle stage of AD. In a related study, Omoluabi et al. (2021) reported no LC cell loss but a reduction in LC fiber density in the piriform cortex and hippocampal DG of htauE14-infused older rats (12 months post-infusions). Surprisingly, at this AD pretangle stage (LC-htauE14 model), GP ROD measurements remained unchanged in htauE14-infused older rats despite LC-NE cell and fibre loss being reported by studies using identical model (Ghosh et al., 2019; Omoluabi et al., 2021).

These observations might imply the presence of compensatory mechanisms in an attempt to maintain homeostasis by counteracting disruption in the LC-NE system as AD progresses. Firstly, increased sprouting of surviving LC neurons in the hippocampus and prefrontal cortex, among other brain regions, is correlated with degeneration of NA system in AD (Szot et al., 2006; Szot et al., 2007). Secondly, Ghosh et al. (2019) observed an upregulation of beta-1 adrenoreceptors concurrent with LC-fiber loss. This concurrent upregulation suggests a compensatory mechanism that potentially contributes to the absence of differences in GP activity found in the current study. Furthermore, AD is associated with increased levels of DβH and tyrosine hydroxylase, the enzyme involved in NE synthesis (Iversen et al., 1983; Miyata et al., 1984; Szot et al., 2006; Szot et al., 2007), which may result in greater production of NE. It has been noted that AD patients have decreased levels of NET (Gulyas et al., 2010). A reduction in NET levels will allow more NE to stay in the synapse because NET mediates NE re-uptake. All these factors (increased NE production, beta-1 adrenoreceptors upregulation, decreased NE absorption and greater neuronal sprouting) may act as compensatory mechanisms in the LC at the early stages of AD. This could account for the absence of GP alterations in the hippocampus at the pretangle stage. Nevertheless, these compensatory mechanisms may not be enough to offset neuronal loss and energy shortages as AD worsens and LC degeneration increases.

4.3 LC-htauE14 Does not Affect GFAP Expression in the Hippocampus of Older Rats

The current study further explored the GFAP profile within the hippocampal subfields to determine whether the relative ROD of GP has a matching astrocytic profile. The main hypothesis that LC-htauE14 infusion would alter the GFAP expression in the hippocampus at the pretangle stage of AD was not supported. The result from the study revealed no effect of LC-

htauE14 infusion and sex on astrocyte expression in the hippocampus of older rats (~20 months p.i.). This implies that ROD measurement of astrocyte GFAP of older animals is not affected by AD condition or sex at the initial stages of AD.

Astrocytes, as essential homeostatic cells in the CNS, are implicated in various neuropathologies (Kulijewicz-Nawrot et al., 2012; Olabarria et al., 2010; Yeh et al., 2011). Their distinctive morphology and spatial arrangement allow them to supply energy substrates from capillaries to neurons (Haber et al., 2006; Kacem et al., 1998). In AD, astrocytes undergo multiple changes at morphological, molecular, and functional levels (Liddelow et al., 2017; Orre et al., 2014). This includes astrocyte atrophy and astrodegeneration, marked by reduced astrocyte volume and surface area in areas such as prefrontal cortex, entorhinal cortex, and hippocampus, as observed in mouse models of AD (Kulijewicz-Nawrot et al., 2012; Olabarria et al., 2010; Yeh et al., 2011).

The results from the present study are consistent with findings reported by Olabarria et al. (2010). They examined GFAP expression in the hippocampus (DG and CA1) of a 3xTg model of AD. Similar to the present study, they reported no effect of AD condition and age on the GFAP density at 6 and 18 months. In addition, Olabarria et al. (2010) observed widespread astrocytic atrophy and reduced surface and volume of GFAP profiles in the hippocampal DG and CA1 at 6 months and 18 months, respectively. The current findings, together with the report from Olabarria et al. (2010), suggest that GFAP ROD remains unaltered at the early stages of AD despite major reductions in its surface area and volume.

The use of older rats in the present study could account for the lack of changes in GFAP ROD in the hippocampus. There is an age-associated reported relocation of GP from astrocytes

to neurons. Drulis-Fajdasz et al. (2018) suggested that the distribution of GP within cells undergoes alterations as animals age. In young animals, it was mainly found in astrocytes, whereas its localization expanded to include both astrocytes and neurons in middle-aged mice (Drulis-Fajdasz et al., 2018). The interaction of age and AD condition on GP and astrocyte profile is lacking. Future studies should therefore investigate these age-associated alterations in energy metabolism among astrocytes and neurons under AD condition. It would be necessary to also measure glycogen content longitudinally in the hippocampus in addition to the volume and surface area of GFAP-stained cells, especially at the pretangle stage. This will enhance our understanding of the overall metabolic alterations occurring throughout AD progression.

4.4 Limitations of the Present Study

While the current findings contribute significantly to filling a void in the existing literature, it is imperative to acknowledge certain limitations when interpreting the results and formulating future studies. Firstly, immunohistochemistry was performed on fresh frozen tissue which may have potential issues with tissue preservation. Although tissues were handled carefully, the risk of possible antigen degradation or loss during freezing and thawing processes as well as decreased antibody penetration caused by the freezing procedure, cannot be overemphasized. Although immunohistochemistry is conventionally performed on fixed tissue for GFAP expression, the current study deemed it crucial to employ matching frozen tissue in tandem with GP analysis, to which immunohistochemical detection is not possible. This allows for examining corresponding sections from the same pair of animals in both GP and astrocytes, mitigating potential issues arising from inter-subject differences that could impact the analysis. Furthermore, I conducted an initial pilot study on GFAP, involving staining and analysis of fresh

frozen and fixed tissues to determine if there are any differences. The ROD measurements from both approaches were found to be identical, justifying the selection of fresh frozen tissue for the study.

Another potential limitation of the present study is that some of the Brightfield images were captured under varying exposure times. Images taken with different exposure times may exhibit variations in illumination levels, which can affect the overall quality and comparability of the captured data. It cannot be determined if this impacted the overall results of the study with certainty. As a result, reimaging and analyses are ongoing to verify the results of the study. A second study analyzing GP and GFAP in a young cohort of LC-tauE14 infused rats 1-3months post infusion is also ongoing, and data will be contrasted with images collected under the same microscope settings. Finally, the results and interpretation of the present study may be limited by the sample size (n = 5 rats/group). However, previous work (Walling et al., 2007) examining prolonged seizure activity in the entorhinal cortex and found similar sample sizes (n = 5-6/group) was sufficient to identify differences.

Conclusion

In conclusion, this research, conducted at the pretangle stage, has determined that LC-htauE14 infusion does not significantly impact GP ROD levels in older rats' hippocampal DG, CA1, and CA3 regions (~20 months p.i). This suggests that the pretangle stage may be too early for observable alterations in energy metabolism or that energy requirements and metabolism may shift with age (Drulis-Fajdasz et al., 2018). The observation of altered GP relative levels in distinct subregions, including the MML, OML, SGZ, CA1 rad, and CA3 pyr, is noteworthy. Assessing glycogen content in these subregions during pretangle occurrence could provide

further insights. While the present study focused on ROD measures of GFAP activity in the hippocampus, future investigations should include other brain regions (beyond the hippocampus) and encompass broader assessments, including astrocyte atrophy, surface area, and volume, to comprehensively understand astrocytic changes during AD and aging.

Lastly, this study did not incorporate an assessment of changes in other enzymatic activities that may occur at the pretangle stage. Understanding potential correlations between glycogen levels, other enzymatic activities, and cognition in AD will be crucial. I propose that AD's glycogen levels may be reduced concurrent with diminished glycogen synthesis and elevated glycogenolysis. Specifically, the upregulation of glycogen synthase kinase 3β (GSK-3β) activity in AD, which inhibits glycogen synthase, could decrease glycogen synthesis (Brown, 2004). However, it is important to note that this was not captured in the current study and warrants dedicated investigation in future studies. This collective approach will enhance our understanding of the intricate interplay between glycogen metabolism, astrocytic changes, and AD progression.

References

Acsády, L., Kamondi, A., Sík, A., Freund, T., & Buzsáki, G. (1998). GABAergic cells are the major postsynaptic targets of mossy fibers in the rat hippocampus. *The Journal of Neuroscience, 18*(9), 3386–3403. https://doi.org/10.1523/JNEUROSCI.18-09-03386.1998

Alzheimer, A., Stelzmann, R. A., Schnitzlein, H. N., & Murtagh, F. R. (1995). An English translation of Alzheimer's 1907 paper, "Uber eine eigenartige Erkankung der Hirnrinde". *Clinical Anatomy (New York, N.Y.), 8*(6), 429–431. https://doi.org/10.1002/ca.980080612

Alzheimer Society of Canada. (n.d.). Dementia numbers in Canada. Retrieved June 2023, from https://alzheimer.ca/en/about-dementia/what-dementia/dementia-numbers-canada

Barbosa, F. F., Pontes, I. M., Ribeiro, S., Ribeiro, A. M., & Silva, R. H. (2012). Differential roles of the dorsal hippocampal regions in the acquisition of spatial and temporal aspects of episodic-like memory. *Behavioural Brain Research, 232*(1), 269–277. https://doi.org/10.1016/j.bbr.2012.04.022

Barnes, L. L., Wilson, R. S., Bienias, J. L., Schneider, J. A., Evans, D. A., & Bennett, D. A. (2005). Sex differences in the clinical manifestations of Alzheimer disease pathology. *Archives of General Psychiatry, 62*(6), 685–691. https://doi.org/10.1001/archpsyc.62.6.685

Bondareff, W., Mountjoy, C. Q., Roth, M., Rossor, M. N., Iversen, L. L., Reynolds, G. P., & Hauser, D. L. (1987). Neuronal degeneration in locus coeruleus and cortical correlates of Alzheimer disease. *Alzheimer Disease and Associated Disorders*, *1*(4), 256–262. https://doi.org/10.1097/00002093-198701040-00005

Braak, H., & Braak, E. (1991). Neuropathological staging of Alzheimer-related changes. *Acta Neuropathologica, 82*(4), 239-259. https://doi.org/10.1007/BF00308809

Braak, R. H., Thal, R. D., Ghebremedhin, R. E., & Del Tredici, R. K. (2011). Stages of the pathologic process in Alzheimer Disease: Age categories from 1 to 100 years. *Journal of Neuropathology and Experimental Neurology, 70*(11), 960-969. https://doi.org/10.1097/NEN.0b013e318232a379

Brown, A. M., Baltan Tekkök, S., & Ransom, B. R. (2004). Energy transfer from astrocytes to axons: the role of CNS glycogen. *Neurochemistry International, 45*(4), 529–536. https://doi.org/10.1016/j.neuint.2003.11.005

Busser, J., Geldmacher, D. S., & Herrup, K. (1998). Ectopic cell cycle proteins predict the sites of neuronal cell death in Alzheimer's disease brain. *The Journal of Neuroscience, 18*(8), 2801-2807. https://doi.org/10.1523/jneurosci.18-08- 02801.1998

Chesler, A., Himwich, H.E., 1944. Effect of insulin hypoglycaemia on glycogen content of parts of the central nervous system of the dog. *Arch. Neurol. Psychiatry, 52*, 114–116.

Cori, G.T., & Cori, C.F. (1945). The Enzymatic Conversion of Phosphorylase a to b. *Journal of Biological Chemistry, 158*, 321-332.

Delacourte, A., David, J. P., Sergeant, N., Buée, L., Wattez, A., Vermersch, P., Ghozali, F., Fallet-Bianco, C., Pasquier, F., Lebert, F., Petit, H., & Di Menza, C. (1999). The biochemical pathway of neurofibrillary degeneration in aging and Alzheimer's disease. *Neurology*, *52(*6), 1158–1165. https://doi.org/10.1212/wnl.52.6.1158

Delatour, B., & Witter, M. P. (2002). Projections from the parahippocampal region to the prefrontal cortex in the rat: evidence of multiple pathways. *The European Journal of Neuroscience, 15*(8), 1400–1407. https://doi.org/10.1046/j.1460-9568.2002.01973.x

de Leon, M. J., Ferris, S. H., George, A. E., Christman, D. R., Fowler, J. S., Gentes, C., Reisberg, B., Gee, B., Emmerich, M., Yonekura, Y., Brodie, J., Kricheff, I. I., & Wolf, A. P. (1983). Positron emission tomographic studies of aging and Alzheimer's disease. *AJNR. American journal of neuroradiology*, *4*(3), 568–571.

Del Tredici, K., Rüb, U., De Vos, R. A., Bohl, J. R., & Braak, H. (2002). Where does Parkinson disease pathology begin in the brain? *Journal of Neuropathology and Experimental neurology*, *61*(5), 413–426. https://doi.org/10.1093/jnen/61.5.413

Dienel, G. A., & Cruz, N. F. (2003). Neighborly interactions of metabolically-activated astrocytes in vivo. *Neurochemistry International*, *43*(4-5), 339–354. https://doi.org/10.1016/s0197-0186(03)00021-4

Dienel, G. A., & Rothman, D. L. (2019). Glycogenolysis in cerebral cortex during sensory stimulation, acute hypoglycemia, and exercise: Impact on astrocytic energetics, aerobic glycolysis, and astrocyte-neuron interactions. *Advances in Neurobiology*, *23*, 209–267. https://doi.org/10.1007/978-3-030-27480-1_8

DiNuzzo, M., Mangia, S., Maraviglia, B., & Giove, F. (2010). Glycogenolysis in astrocytes supports blood-borne glucose channeling not glycogen-derived lactate shuttling to neurons: evidence from mathematical modeling. *Journal of Cerebral Blood Flow and Metabolism, 30*(12), 1895–1904. https://doi.org/10.1038/jcbfm.2010.151

Drechsel, D. N., Hyman, A. A., Cobb, M. H., & Kirschner, M. W. (1992). Modulation of the dynamic instability of tubulin assembly by the microtubule-associated protein tau. *Molecular Biology of the Cell*, *3*(10), 1141–1154. https://doi.org/10.1091/mbc.3.10.1141

Drulis-Fajdasz, D., Gizak, A., Wójtowicz, T., Wiśniewski, J. R., & Rakus, D. (2018). Aging-associated changes in hippocampal glycogen metabolism in mice. Evidence for and against astrocyte-to-neuron lactate shuttle. *Glia, 66*(7*),* 1481–1495. https://doi.org/10.1002/glia.23319

Dubal, D. B., Broestl, L., & Worden, K. (2012). Sex and gonadal hormones in mouse models of Alzheimer's disease: what is relevant to the human condition*? Biology of Sex Differences, 3*(1), 24. https://doi.org/10.1186/2042-6410-3-24

Evans, D. A., Funkenstein, H. H., Albert, M. S., Scherr, P. A., Cook, N. R., Chown, M. J., Hebert, L. E., Hennekens, C. H., & Taylor, J. O. (1989). Prevalence of Alzheimer's disease in a community population of older persons. Higher than previously reported. *JAMA*, *262*(18), 2551–2556.

Filon, J. R., Intorcia, A. J., Sue, L. I., Vazquez Arreola, E., Wilson, J., Davis, K. J., Sabbagh, M. N., Belden, C. M., Caselli, R. J., Adler, C. H., Woodruff, B. K., Rapscak, S. Z., Ahern, G. L., Burke, A. D., Jacobson, S., Shill, H. A., Driver-Dunckley, E., Chen, K., Reiman, E. M., Beach, T. G., … Serrano, G. E. (2016). Gender differences in Alzheimer's Disease: Brain atrophy, histopathology burden, and cognition. *Journal of Neuropathology and Experimental Neurology, 75*(8), 748–754. https://doi.org/10.1093/jnen/nlw047

Fischer, E. H., & Krebs, E. G. (1955). Conversion of phosphorylase b to phosphorylase a in muscle extracts. *The Journal of Biological Chemistry*, *216*(1), 121–132.

Gale, S. D., Baxter, L., & Thompson, J. (2016). Greater memory impairment in dementing females than males relative to sex-matched healthy controls. *Journal of Clinical and Experimental Neuropsychology, 38*(5), 527–533. https://doi.org/10.1080/13803395.2015.1132298

Garcia-Alloza, M., Robbins, E. M., Zhang-Nunes, S. X., Purcell, S. M., Betensky, R. A., Raju, S., Prada, C., Greenberg, S. M., Bacskai, B. J., & Frosch, M. P. (2006). Characterization of amyloid deposition in the APPswe/PS1dE9 mouse model of Alzheimer disease. *Neurobiology of Disease, 24*(3), 516–524.

Ghosh, A., Torraville, S. E., Mukherjee, B., Walling, S. G., Martin, G. M., Harley, C. W., & Yuan, Q. (2019). An experimental model of Braak's pretangle proposal for the origin of Alzheimer's disease: the role of locus coeruleus in early symptom development. *Alzheimer's Research & Therapy, 11*(1), 59.

Giaume, C., Kirchhoff, F., Matute, C., Reichenbach, A., & Verkhratsky, A. (2007). Glia: the fulcrum of brain diseases. *Cell Death and Differentiation*, *14*(7), 1324–1335. https://doi.org/10.1038/sj.cdd.4402144

Gibbs, M. E., Anderson, D. G., & Hertz, L. (2006). Inhibition of glycogenolysis in astrocytes interrupts memory consolidation in young chickens. *Glia, 54*(3), 214–222. https://doi.org/10.1002/glia.20377

Gibbs, M. E., O'dowd, B. S., Hertz, E., & Hertz, L. (2006). Astrocytic energy metabolism consolidates memory in young chicks. *Neuroscience, 141* (1), 9–13. https://doi.org/10.1016/j.neuroscience.2006.04.038

Glenner, G. G., & Wong, C. W. (1984). Alzheimer's disease: initial report of the purification and characterization of a novel cerebrovascular amyloid protein. *Biochemical and*

Biophysical Research Communications, 120(3), 885–890. https://doi.org/10.1016/s0006-291x(84)80190-4

Gulyás, B., Brockschnieder, D., Nag, S., Pavlova, E.L., Kása, P., Beliczai, Z., Legradi, A., Gulya, K., Thiele, A., Dyrks, T., & Halldin, C. (2010). The norepinephrine transporter (NET) radioligand (S,S)-[18F]FMeNER-D2 shows significant decreases in NET density in the human brain in Alzheimer's disease: A post-mortem autoradiographic study. *Neurochemistry International, 56*, 789-798.

Haber, M., Zhou, L., & Murai, K. K. (2006). Cooperative astrocyte and dendritic spine dynamics at hippocampal excitatory synapses. *The Journal of neuroscience, 26*(35), 8881–8891. https://doi.org/10.1523/JNEUROSCI.1302-06.2006

Hampel, H., & Broich, K. (2009). Enrichment of MCI and early Alzheimer's disease treatment trials using neurochemical and imaging candidate biomarkers. *The journal of Nutrition, Health and Aging, 13*(4), 373–375. https://doi.org/10.1007/s12603-009-0048-3

Hendrie, H. C., Osuntokun, B. O., Hall, K. S., Ogunniyi, A. O., Hui, S. L., Unverzagt, F. W., Gureje, O., Rodenberg, C. A., Baiyewu, O., & Musick, B. S. (1995). Prevalence of Alzheimer's disease and dementia in two communities: Nigerian Africans and African Americans. *The American Journal of Psychiatry*, *152*(10), 1485–1492. https://doi.org/10.1176/ajp.152.10.1485

Heneka, M. T., Nadrigny, F., Regen, T., Martinez-Hernandez, A., Dumitrescu-Ozimek, L., Terwel, D., Jardanhazi-Kurutz, D., Walter, J., Kirchhoff, F., Hanisch, U. K., & Kummer, M. P. (2010). Locus ceruleus controls Alzheimer's disease pathology by modulating microglial functions through norepinephrine. *Proceedings of the National Academy of Sciences of the United States of America, 107*(13), 6058–6063. https://doi.org/10.1073/pnas.0909586107

Hua, X., Hibar, D. P., Lee, S., Toga, A. W., Jack, C. R., Jr, Weiner, M. W., Thompson, P. M., & Alzheimer's Disease Neuroimaging Initiative (2010). Sex and age differences in atrophic rates: an ADNI study with n=1368 MRI scans. *Neurobiology of Aging, 31*(8), 1463–1480. https://doi.org/10.1016/j.neurobiolaging.2010.04.033

Iqbal, K., Liu, F., Gong, C. X., Alonso, A.delC., & Grundke-Iqbal, I. (2009). Mechanisms of tau-induced neurodegeneration. *Acta Neuropathologica, 118*(1), 53–69. https://doi.org/10.1007/s00401-009-0486-3

Iqbal, K., Zaidi, T., Wen, G. Y., Grundke-Iqbal, I., Merz, P. A., Shaikh, S. S., Wisniewski, H. M., AlafuzofT, I., & Winblad, B. (1987). Defective brain microtubule assembly in Alzheimer's disease. *Alzheimer Disease and Associated Disorders, 1*(3), 201-202. https://doi.org/10.1097/00002093-198701030-00017

Iversen, L. L., Rossor, M. N., Reynolds, G. P., Hills, R., Roth, M., Mountjoy, C. Q., Foote, S. L., Morrison, J. H., & Bloom, F. E. (1983). Loss of pigmented dopamine-beta-hydroxylase positive cells from locus coeruleus in senile dementia of Alzheimer's type. *Neuroscience Letters*, *39*(1), 95–100. https://doi.org/10.1016/0304-3940(83)90171-4

Johnson, K. A., Schultz, A., Betensky, R. A., Becker, J. A., Sepulcre, J., Rentz, D., Mormino, E., Chhatwal, J., Amariglio, R., Papp, K., Marshall, G., Albers, M., Mauro, S., Pepin, L., Alverio, J., Judge, K., Philiossaint, M., Shoup, T., Yokell, D., Dickerson, B., … Sperling, R. (2016). Tau positron emission tomographic imaging in aging and early Alzheimer disease. *Annals of Neurology*, *79*(1), 110–119. https://doi.org/10.1002/ana.24546

Kacem, K., Lacombe, P., Seylaz, J., & Bonvento, G. (1998). Structural organization of the perivascular astrocyte endfeet and their relationship with the endothelial glucose transporter: a confocal microscopy study. *Glia*, *23*(1), 1–10.

Kandel E.R., & Schwartz J.H., & Jessell T.M., & Siegelbaum S.A., & Hudspeth A.J., & Mack S(Eds.), (2014). *Principles of Neural Science, Fifth Edition*. McGraw Hill.

Karttunen, K., Karppi, P., Hiltunen, A., Vanhanen, M., Välimäki, T., Martikainen, J., Valtonen, H., Sivenius, J., Soininen, H., Hartikainen, S., Suhonen, J., Pirttilä, T., & ALSOVA study group (2011). Neuropsychiatric symptoms and quality of life in patients with very mild and mild Alzheimer's disease. *International Journal of Geriatric Psychiatry, 26*(5), 473–482. https://doi.org/10.1002/gps.2550

Kitamura, T., Kitamura, M., Hino, S., Tanaka, N., & Kurata, K. (2012). Gender differences in clinical manifestations and outcomes among hospitalized patients with behavioral and psychological symptoms of dementia. *The Journal of Clinical Psychiatry, 73*(12), 1548–1554. https://doi.org/10.4088/JCP.11m07614

Kulijewicz-Nawrot, M., Verkhratsky, A., Chvátal, A., Syková, E., & Rodríguez, J. J. (2012). Astrocytic cytoskeletal atrophy in the medial prefrontal cortex of a triple transgenic mouse model of Alzheimer's disease. *Journal of Anatomy, 221*(3), 252–262. https://doi.org/10.1111/j.1469-7580.2012.01536.x

Lethbridge, R. L., Walling, S. G., & Harley, C. W. (2014). Modulation of the perforant path-evoked potential in dentate gyrus as a function of intrahippocampal β- adrenoceptor agonist concentration in urethane-anesthetized rat. *Brain and Behavior, 4*(1), 95-103. https://doi.org/10.1002/brb3.199

Liddelow, S. A., Guttenplan, K. A., Clarke, L. E., Bennett, F. C., Bohlen, C. J., Schirmer, L., Bennett, M. L., Münch, A. E., Chung, W. S., Peterson, T. C., Wilton, D. K., Frouin, A., Napier, B. A., Panicker, N., Kumar, M., Buckwalter, M. S., Rowitch, D. H., Dawson, V.

L., Dawson, T. M., Stevens, B., … Barres, B. A. (2017). Neurotoxic reactive astrocytes are induced by activated microglia. *Nature, 541*(7638), 481–487. https://doi.org/10.1038/nature21029

Lin, K. A., Choudhury, K. R., Rathakrishnan, B. G., Marks, D. M., Petrella, J. R., Doraiswamy, P. M., & Alzheimer's Disease Neuroimaging Initiative (2015). Marked gender differences in progression of mild cognitive impairment over 8 years. *Alzheimer's & Dementia (New York, N. Y.), 1*(2), 103–110. https://doi.org/10.1016/j.trci.2015.07.001

Magistretti, P. J., & Pellerin, L. (1996). Cellular mechanisms of brain energy metabolism. Relevance to functional brain imaging and to neurodegenerative disorders. *Annals of the New York Academy of Sciences*, *777*, 380–387. https://doi.org/10.1111/j.1749-6632.1996.tb34449.x

Magistretti, P.J., Sorg, O., & Martin, J.L. (1993). Regulation of glycogen metabolism in astrocytes: physiological, pharmacological, and pathological aspects. *In Astrocytes: Pharmacology and Function, S. Murphy, ed. (San Diego: Academic Press)*, pp. 243–265

Malpetti, M., Ballarini, T., Presotto, L., Garibotto, V., Tettamanti, M., Perani, D., Alzheimer's Disease Neuroimaging Initiative (ADNI) database, & Network for Efficiency and Standardization of Dementia Diagnosis (NEST-DD) database (2017). Gender differences in healthy aging and Alzheimer's Dementia: A 18 F-FDG-PET study of brain and cognitive reserve. *Human brain mapping, 38*(8), 4212–4227. https://doi.org/10.1002/hbm.23659

Mann, D. M., Sumpter, P. Q., Davies, C. A., & Yates, P. O. (1987). Glycogen accumulations in the cerebral cortex in Alzheimer's disease. *Acta neuropathologica*, *73*(2), 181–184. https://doi.org/10.1007/BF00693786

Matthews, K. L., Chen, C. P., Esiri, M. M., Keene, J., Minger, S. L., & Francis, P. T. (2002). Noradrenergic changes, aggressive behavior, and cognition in patients with dementia. *Biological psychiatry*, *51*(5), 407–416. https://doi.org/10.1016/s0006-

Matsui, T., Ishikawa, T., Ito, H., Okamoto, M., Inoue, K., Lee, M. C., Fujikawa, T., Ichitani, Y., Kawanaka, K., & Soya, H. (2012). Brain glycogen supercompensation following exhaustive exercise. *The Journal of Physiology, 590*(3), 607–616. https://doi.org/10.1113/jphysiol.2011.217919

Mattsson, N., Lönneborg, A., Boccardi, M., Blennow, K., Hansson, O., & Geneva Task Force for the Roadmap of Alzheimer's Biomarkers (2017). Clinical validity of cerebrospinal fluid Aβ42, tau, and phospho-tau as biomarkers for Alzheimer's disease in the context of a structured 5-phase development framework. *Neurobiology of Aging, 52*, 196–213. https://doi.org/10.1016/j.neurobiolaging.2016.02.034

Mega, M. S., Cummings, J. L., Fiorello, T., & Gornbein, J. (1996). The spectrum of behavioral changes in Alzheimer's disease. *Neurology, 46*(1), 130–135. https://doi.org/10.1212/wnl.46.1.130

Meijer A. E. (1968). Improved histochemical method for the demonstration of the activity of alpha-glucan phosphorylase. The use of glucosyl acceptor dextran. *Histochemie. Histochemistry*, *12*(3), 244–252. https://doi.org/10.1007/BF00306002

Miyata, S., Nagata, H., Yamao, S., Nakamura, S., & Kameyama, M. (1984). Dopamine-β-hydroxylase activities in serum and cerebrospinal fluid of aged and demented patients. *Journal of the Neurological Sciences, 63*, 403-409.

Morgello, S., Uson, R. R., Schwartz, E. J., & Haber, R. S. (1995). The human blood-brain barrier glucose transporter (GLUT1) is a glucose transporter of gray matter astrocytes. *Glia*, *14*(1), 43–54. https://doi.org/10.1002/glia.440140107

Mosconi, L., Mistur, R., Switalski, R., Tsui, W. H., Glodzik, L., Li, Y., Pirraglia, E., De Santi, S., Reisberg, B., Wisniewski, T., & de Leon, M. J. (2009). FDG-PET changes in brain glucose metabolism from normal cognition to pathologically verified Alzheimer's disease. *European Journal of Nuclear Medicine and Molecular Imaging, 36*(5), 811–822. https://doi.org/10.1007/s00259-008-1039-zx

Nakashiba, T., Buhl, D. L., McHugh, T. J., & Tonegawa, S. (2009). Hippocampal CA3 output is crucial for ripple-associated reactivation and consolidation of memory. *Neuron, 62*(6), 781–787. https://doi.org/10.1016/j.neuron.2009.05.013

Nelson, T., Kaufman, E. E., & Sokoloff, L. (1984). 2-Deoxyglucose incorporation into rat brain glycogen during measurement of local cerebral glucose utilization by the 2-deoxyglucose method. *Journal of Neurochemistry*, *43*(4), 949–956.

Newman, L. A., Korol, D. L., & Gold, P. E. (2011). Lactate produced by glycogenolysis in astrocytes regulates memory processing. *PloS One*, *6*(12), e28427. https://doi.org/10.1371/journal.pone.00284276), 336–342.

Olabarria, M., Noristani, H. N., Verkhratsky, A., & Rodríguez, J. J. (2010). Concomitant astroglial atrophy and astrogliosis in a triple transgenic animal model of Alzheimer's disease. *Glia, 58*(7), 831–838. https://doi.org/10.1002/glia.20967

Omoluabi, T., Torraville, S. E., Maziar, A., Ghosh, A., Power, K. D., Reinhardt, C., Harley, C. W., & Yuan, Q. (2021). Novelty-like activation of locus coeruleus protects against deleterious human pretangle tau effects while stress-inducing activation worsens its effects. *Alzheimer's & Dementia (New York, N. Y.)*, *7*(1), e12231. https://doi.org/10.1002/trc2.12231

Orre, M., Kamphuis, W., Osborn, L. M., Jansen, A. H. P., Kooijman, L., Bossers, K., & Hol, E. M. (2014). Isolation of glia from Alzheimer's mice reveals inflammation and dysfunction. *Neurobiology of Aging, 35*(12), 2746–2760. https://doi.org/10.1016/j.neurobiolaging.2014.06.004

Plaschke, K., & Hoyer, S. (1993). Action of the diabetogenic drug streptozotocin on glycolytic and glycogenolytic metabolism in adult rat brain cortex and hippocampus. *International Journal of Developmental Neuroscience, 11(4),* 477–483. https://doi.org/10.1016/0736-5748(93)90021-5

Pellerin, L., & Magistretti, P. J. (1994). Glutamate uptake into astrocytes stimulates aerobic glycolysis: a mechanism coupling neuronal activity to glucose utilization. *Proceedings of the National Academy of Sciences of the United States of America*, *91*(22), 10625–10629. https://doi.org/10.1073/pnas.91.22.10625

Perry, R. J. (1999). Attention and executive deficits in Alzheimer's disease: A critical review. *Brain, 122*(3), 383-404. https://doi.org/10.1093/brain/122.3.383

Price, J.L. and Morris, J.C. (1999), Tangles and plaques in nondemented aging and "preclinical" Alzheimer's disease. *Ann Neurol., 45*, 358-368.

Reisberg, B., Ferris, S. H., de Leon, M. J., & Crook, T. (1982). The Global Deterioration Scale for assessment of primary degenerative dementia. *The American Journal of Psychiatry*, *139*(9), 1136–1139. https://doi.org/10.1176/ajp.139.9.1136

Schlichting, M. L., Zeithamova, D., & Preston, A. R. (2014). CA1 subfield contributions to memory integration and inference. *Hippocampus, 24*(10), 1248–1260

Seifert, G., Schilling, K., & Steinhäuser, C. (2006). Astrocyte dysfunction in neurological disorders: a molecular perspective. *Nature Reviews. Neuroscience*, *7*(3), 194–206. https://doi.org/10.1038/nrn1870

Shinohara, M., Murray, M. E., Frank, R. D., Shinohara, M., DeTure, M., Yamazaki, Y., Tachibana, M., Atagi, Y., Davis, M. D., Liu, C. C., Zhao, N., Painter, M. M., Petersen, R. C., Fryer, J. D., Crook, J. E., Dickson, D. W., Bu, G., & Kanekiyo, T. (2016). Impact of sex and APOE4 on cerebral amyloid angiopathy in Alzheimer's disease. *Acta Neuropathologica, 132*(2), 225–234. https://doi.org/10.1007/s00401-016-1580-y

Skup, M., Zhu, H., Wang, Y., Giovanello, K. S., Lin, J. A., Shen, D., Shi, F., Gao, W., Lin, W., Fan, Y., Zhang, H., & Alzheimer's Disease Neuroimaging Initiative (2011). Sex differences in grey matter atrophy patterns among AD and aMCI patients: results from ADNI. *NeuroImage, 56*(3), 890–906. https://doi.org/10.1016/j.neuroimage.2011.02.060

Sokoloff L. (1999). Energetics of functional activation in neural tissues. *Neurochemical Research*, *24*(2), 321–329. https://doi.org/10.1023/a:1022534709672

Suzuki, A., Stern, S. A., Bozdagi, O., Huntley, G. W., Walker, R. H., Magistretti, P. J., & Alberini, C. M. (2011). Astrocyte-neuron lactate transport is required for long-term memory formation. *Cell, 144*(5), 810–823. https://doi.org/10.1016/j.cell.2011.02.018

Swanson, R.A., Morton, M.M., Sagar, S.M., Sharp, F.R., (1992). Sensory stimulation induces local cerebral glycogenolysis: demonstration by autoradiography. *Neuroscience 51*, 451–461.

Szot, P., White, S. S., Greenup, J. L., Leverenz, J. B., Peskind, E. R., & Raskind, M. A. (2006). Compensatory changes in the noradrenergic nervous system in the locus coeruleus and hippocampus of postmortem subjects with Alzheimer's disease and dementia with Lewy bodies. *The Journal of Neuroscience*, *26*(2), 467–478. https://doi.org/10.1523/JNEUROSCI.4265-05.2006

Szot, P., White, S. S., Greenup, J. L., Leverenz, J. B., Peskind, E. R., & Raskind, M. A. (2007). Changes in adrenoreceptors in the prefrontal cortex of subjects with dementia: evidence of compensatory changes. *Neuroscience*, *146*(1), 471–480. https://doi.org/10.1016/j.neuroscience.2007.01.031

Tensil, M., Hessler, J. B., Gutsmiedl, M., Riedl, L., Grimmer, T., & Diehl-Schmid, J. (2018). Sex Differences in Neuropsychological Test Performance in Alzheimer's Disease and the Influence of the ApoE Genotype. *Alzheimer Disease and Associated Disorders, 32*(2), 145–149. https://doi.org/10.1097/WAD.0000000000000229

Walling, S. G., Bromley, K., & Harley, C. W. (2006). Glycogen phosphorylase reactivity in the entorhinal complex in familiar and novel environments: evidence for labile glycogenolytic modules in the rat. *Journal of Chemical Neuroanatomy, 31*(2), 108–113. https://doi.org/10.1016/j.jchemneu.2005.09.004

Walling, S. G., Rigoulot, A., & Scharfman, H. E. (2007). Acute and chronic changes in glycogen phosphorylase in hippocampus and entorhinal cortex after status epilepticus in the adult male rat. *The European Journal of Neuroscience*, *26*(1), 178. https://doi.org/10.1111/j.1460-9568.2007.05657.x

Wilhelmsson, U., Bushong, E. A., Price, D. L., Smarr, B. L., Phung, V., Terada, M., Ellisman, M. H., & Pekny, M. (2006). Redefining the concept of reactive astrocytes as cells that

remain within their unique domains upon reaction to injury. *Proceedings of the National Academy of Sciences of the United States of America*, *103*(46), 17513–17518. https://doi.org/10.1073/pnas.0602841103

World Health Organization. (2021). Dementia. Retrieved from https://www.who.int/news-room/fact-sheets/detail/dementia

Yeh, C. Y., Vadhwana, B., Verkhratsky, A., & Rodríguez, J. J. (2011). Early astrocytic atrophy in the entorhinal cortex of a triple transgenic animal model of Alzheimer's disease. *ASN neuro, 3*(5), 271–279. https://doi.org/10.1042/AN20110025

Yue, M., Hanna, A., Wilson, J., Roder, H., & Janus, C. (2011). Sex difference in pathology and memory decline in rTg4510 mouse model of tauopathy. *Neurobiology of Aging, 32*(4), 590–603. https://doi.org/10.1016/j.neurobiolaging.2009.04.006

Zilka, N., & Novak, M. (2006). The tangled story of Alois Alzheimer. *Bratislavske Lekarske Listy, 107*(9-10), 343–345.